Spectral properties of a two-orbital Anderson impurity model across a non-Fermi-liquid fixed point

Lorenzo De Leo[1] and Michele Fabrizio[1,2]
[1]*International School for Advanced Studies (SISSA), and Istituto Nazionale per la Fisica della Materia (INFM) UR-Trieste SISSA, Via Beirut 2-4, I-34014 Trieste, Italy*
[2]*The Abdus Salam International Center for Theoretical Physics (ICTP), P.O.Box 586, I-34014 Trieste, Italy*
(Received 4 February 2004; revised manuscript received 29 March 2004; published 25 June 2004)

We study by Wilson numerical renormalization group the spectral properties of a two-orbital Anderson impurity model in the presence of an exchange splitting that follows either regular or inverted Hund's rules. The phase diagram contains a non-Fermi-liquid fixed point separating a screened phase, where conventional Kondo effect occurs, from an unscreened one, where the exchange splitting takes care of quenching the impurity degrees of freedom. On the Kondo screened side close to this fixed point the impurity density of states shows a narrow Kondo peak on top of a broader resonance. This narrow peak transforms in the unscreened phase into a narrow pseudogap inside the broad resonance. Right at the fixed point only the latter survives. The fixed point is therefore identified by a jump of the density of states at the chemical potential. We also consider the effect of several particle-hole symmetry-breaking terms. We show that particle-hole perturbations that simply shift the orbital energies do not wash out the fixed point, unlike those perturbations that hybridize the two orbitals. Consequently the density-of-state jump at the chemical potential remains finite even away from particle-hole symmetry. In other words, the pseudogap stays pinned at the chemical potential, although it is partially filled in. We also discuss the relevance of these results for lattice models that map onto this Anderson impurity model in the limit of large lattice coordination. Upon approaching the Mott metal-insulator transition, these lattice models necessarily enter a region with a local criticality that reflects the impurity non-Fermi-liquid fixed point. However, unlike the impurity, the lattice can get rid of the single-impurity fixed-point instability by spontaneously developing bulk coherent symmetry-broken phases, which we identify for different lattice models.

DOI: 10.1103/PhysRevB.69.245114 PACS number(s): 71.30.+h, 72.15.Qm, 71.10.Hf, 74.20.Mn

I. INTRODUCTION

Non-Fermi-liquid behavior may emerge in Anderson and Kondo impurity models for two distinct reasons. The first one is that, by construction, the conduction electrons may not be able to perfectly screen the impurity degrees of freedom for the Kondo effect. This is realized, for instance, in multichannel Kondo models.[1]

The alternative route towards non-Fermi-liquid behavior is the presence of an intra-impurity mechanism that splits the impurity degeneracy favoring a nondegenerate configuration. The Kondo exchange takes advantage of letting the impurity tunnel among all available electronic configurations. This quantum tunneling is hampered by any term that splits the degeneracy and tends to trap the impurity into a given state. Therefore either the Kondo exchange overwhelms the intra-impurity splitting mechanism or vice versa, which leads, respectively, to a Kondo-screened phase or an unscreened phase. When none of the two effects prevails, a nontrivial behavior may appear. This is actually what happens in the two $S=1/2$ impurity Kondo model in the presence of an antiferromagnetic direct exchange between impurity spins.[2,3] There it is known that, under particular circumstances,[4] an unstable non-Fermi-liquid fixed point separates the Kondo-screened and unscreened regimes. Since this fixed point requires fine tuning of the model parameters, it is tempting to conclude that it is of little physical relevance. In reality a similar competition may be at the heart of strongly correlated electron lattice models. Here the kinetic energy profits by the electrons hopping coherently through the whole lattice. In contrast, the strong correlation tries to optimize on-site (atomic) energetics, thus opposing the hopping. This may involve two energy scales. The higher one is the so-called Hubbard U, which tends to suppress on-site valence fluctuations. The lower one, let us call it J, governs the splitting among on-site electronic configurations at fixed charge. It may be controlled by the exchange splitting, by the crystal field, by local distortion modes, or even by short-range intersite correlations. When the lattice model is driven towards a Mott metal-insulator transition (MIT), either by increasing U or by doping at large U, it necessarily encounters a regime in which the coherent quasiparticle bandwidth W_{qp} is of the same order as J, which we expect is essentially unaffected by U as it just determines the multiplet splitting at fixed charge. Since coherent hopping tends to occupy more or less democratically all multiplets, it opposes J. Out of this competition interesting physical properties may emerge, just like in the Anderson impurity models we discussed before. The analogy between the impurity and the lattice models can be even put on firm grounds in the limit of large coordination lattices through dynamical mean field theory (DMFT).[5] In that limit it is possible to map the lattice model into an effective Anderson impurity model (AIM) subject to a self-consistency condition that relates the impurity Green's function to the hybridization with the conduction bath. The quasiparticle bandwidth of the lattice model transforms into the

Kondo temperature T_K of the AIM. Since approaching the MIT $W_{qp}\to 0$, the effective AIM is necessarily driven into the regime $T_K \sim J$, where the competition among the two screening mechanisms may result in anomalous physical properties. Exactly this competition was invoked by Ref. 6 to explain the appearance of a superconducting pocket, later shown to have a hugely enhanced superconducting gap,[7] just before the MIT in a model for alkali-metal-doped fullerenes.

More recently we have demonstrated by Wilson numerical renormalization group and by bosonization that a twofold orbitally degenerate AIM in the presence of inverted Hund's rules possesses a non-Fermi-liquid unstable fixed point similar to the two-impurity Kondo model one.[8] Because of the aforementioned reasons, any lattice model that maps by DMFT into the same AIM should necessarily meet this fixed point on the route towards a MIT. We argued that, unlike the single-impurity model, those lattice models might spontaneously generate, by the DMFT self-consistency conditions, a bulk order parameter to get rid of the single-impurity fixed-point instability. Since the fixed point is unstable in different particle-hole and particle-particle channels, there exist in principle several competing bulk instabilities. We speculated that, in the absence of nesting or band-structure singularities, the most likely instability is towards superconductivity. These predictions have been just recently confirmed on a lattice model by a DMFT calculation.[9] In this paper we pursue the analysis of that AIM by uncovering the spectral behavior across the non-Fermi-liquid fixed point. This is not only interesting of the AIM itself, being one of the few cases where non-Fermi-liquid dynamical properties may be accessed, but also in the context of the DMFT mapping. The model is also sufficiently simple to allow for an analytical description of the spectral function that reproduces well the numerical results and provides new physical insights. Actually our model spectral function has been quite useful in guiding the analysis of the DMFT solution presented in Ref. 9.

The paper is organized as follows. In Sec. II we describe the two-orbital AIM model. In Sec. III we introduce three lattice models that map by DMFT onto the two-orbital AIM: (a) a two-band Hubbard model with $e\otimes E$ Jahn-Teller coupling to local phonons; (b) a two-band Hubbard model in the presence of single-ion anisotropy; (c) two coupled Hubbard planes. In Sec. IV we review in more detail the Wilson numerical renormalization group calculations of Ref. 8 and present an analysis based on Fermi-liquid theory, which we develop in the Appendix. The results concerning the dynamical properties are presented in Sec. V. In Sec. VI we extract from the numerical data an analytical expression of the impurity spectral function. The role of symmetry-breaking terms in particle-hole channels is investigated in Sec. VII. Conclusions are presented in Sec. VIII.

II. THE MODEL HAMILTONIAN

The AIM Hamiltonian we consider is

$$H = H_U + H_J + H_c + H_{hyb} = \frac{U}{2}(n_d - 2 + \nu)^2 + 2J[(T^x)^2 + (T^y)^2] + \sum_{\mathbf{k}a\alpha} \epsilon_{\mathbf{k}} c^\dagger_{\mathbf{k}a\alpha} c_{\mathbf{k}a\alpha} + \sum_{\mathbf{k}a\alpha} V_d (c^\dagger_{\mathbf{k}a\alpha} d_{a\alpha} + d^\dagger_{a\alpha} c_{\mathbf{k}a\alpha}). \quad (1)$$

Here $c^\dagger_{\mathbf{k}a\alpha}$ creates a conduction electron in the band $a=1,2$ with momentum $\mathbf{k}$, spin α, and energy $\epsilon_{\mathbf{k}}$, measured with respect to the chemical potential. $d^\dagger_{a\alpha}$ is the creation operator of an electron with spin α in the impurity orbital $a=1,2$, while $n_d=\Sigma_{a\alpha} d^\dagger_{a\alpha} d_{a\alpha}$ is the impurity occupation number. We have defined the orbital pseudospin operators

$$T^i = \frac{1}{2}\sum_\alpha \sum_{a=1,2} d^\dagger_{a\alpha} \tau^i_{ab} d_{b\alpha}, \quad (2)$$

where $i=x,y,z$ and τ^i's are the Pauli matrices in the orbital space. We further assume that the conduction band density of states is symmetric with respect to the chemical potential, set equal to zero, so that the behavior of the Hamiltonian under a particle-hole symmetry transformation is controlled by the parameter ν in Eq. (1). For the time being we will take $\nu=0$, which implies that the Hamiltonian is particle-hole symmetric. Afterwards we will release this constraint. The model without the impurity exchange coupling J is SU(4) invariant. A finite J lowers the SU(4) symmetry down to $\mathrm{SU}(2)_{spin}\times \mathrm{O}(2)_{orbit}$. In this case the total charge, the total spin, and the total z-component of the pseudospin are the only conserved quantities.

It is convenient to start our analysis with the spectrum of the isolated impurity, $V_d=0$. The impurity eigenstates, $|n,S,S^z,T,T^z\rangle$, can be labeled by the occupation number n, the spin S, pseudospin T, and their z components, S^z and T^z, respectively, with energies

$$E(n,S,S^z,T,T^z) = \frac{U}{2}(n-2)^2 + 2J[T(T+1) - (T^z)^2]. \quad (3)$$

We assume $U \gg |J|$, so that the impurity ground state with $\nu=0$ has $n=2$. In this case the only configurations allowed by Pauli principle are a spin triplet pseudospin singlet, $S=1$ and $T=0$,

$$|2,1,+1,0,0\rangle = d^\dagger_{1\uparrow} d^\dagger_{2\uparrow} |0\rangle,$$

$$|2,1,0,0,0\rangle = \frac{1}{\sqrt{2}}(d^\dagger_{1\uparrow} d^\dagger_{2\downarrow} - d^\dagger_{2\uparrow} d^\dagger_{1\downarrow})|0\rangle,$$

$$|2,1,-1,0,0\rangle = d^\dagger_{1\downarrow} d^\dagger_{2\downarrow} |0\rangle, \quad (4)$$

and a spin singlet pseudospin triplet, $S=0$ and $T=1$. The latter is split by J into a singlet with $T^z=0$,

$$|2,0,0,1,0\rangle = \frac{1}{\sqrt{2}}(d^\dagger_{1\uparrow} d^\dagger_{2\downarrow} + d^\dagger_{2\uparrow} d^\dagger_{1\downarrow})|0\rangle, \quad (5)$$

and a doublet with $T^z=\pm 1$,

$$|2,0,0,1,+1\rangle = d^\dagger_{1\uparrow} d^\dagger_{1\downarrow} |0\rangle,$$

$$|2,0,0,1,-1\rangle = d^{\dagger}_{2\uparrow} d^{\dagger}_{2\downarrow} |0\rangle. \tag{6}$$

If $J>0$, the lowest-energy configuration is the spin triplet, $S=1$ and $T=0$, which corresponds to the conventional Hund's rules. In contrast, for $J<0$, the isolated impurity ground state is the singlet (5) with quantum numbers $S=0$, $T=1$, and $T^z=0$. We postpone to the following section a discussion about physical realization of such inverted Hund's rules.

A finite hybridization, $V_d \neq 0$, induces valence fluctuations within the impurity, which are controlled by the energy scale (hybridization width)

$$\Delta_0 = \pi\, V_d^2\, \rho_c, \tag{7}$$

with ρ_c the conduction electron density of states (DOS) at the chemical potential per spin and band. These fluctuations are suppressed by a strong repulsion $U \gg \Delta_0$, which we assume throughout this work. Although all our calculations refer to the AIM (1), it is more insightful to discuss some physical properties in terms of the effective Kondo model which describes the low-energy behavior when $U \gg \Delta_0$:

$$H_{eff} = H_J + H_c + H_K, \tag{8}$$

where H_J and H_c have been defined in Eq. (1) and the Kondo exchange

$$H_K = J_K \left[\vec{S}\cdot\vec{\mathcal{S}} + \vec{T}\cdot\vec{\mathcal{T}} + 4 \sum_{i,j=x,y,z} W_{ij}\, \mathcal{W}_{ij} \right], \tag{9}$$

with

$$J_K = 2V_d^2/U. \tag{10}$$

Here $\vec{S}$, defined by

$$\vec{S} = \frac{1}{2} \sum_a \sum_{\alpha\beta} d^{\dagger}_{a\alpha}\, \vec{\sigma}_{\alpha\beta}\, d_{a\beta},$$

$\vec{T}$, which we introduced in Eq. (2), and W_{ij},

$$W_{ij} = \frac{1}{4} \sum_{ab} \sum_{\alpha\beta} d^{\dagger}_{a\alpha}\, \tau^i_{ab}\, \sigma^j_{\alpha\beta}\, d_{b\beta},$$

are impurity spin, pseudospin, and spin-orbital operators, respectively, while $\vec{\mathcal{S}}$, $\vec{\mathcal{T}}$, and $\mathcal{W}_{ij}$ are the corresponding conduction electron density operators at the impurity site. The impurity operators in Eq. (9) act only in the subspace with two electrons occupying the *d* orbitals, which, as we showed, includes six states. The Kondo model (8) contains two competing mechanisms that tend to freeze the leftover impurity degrees of freedom: (i) the Kondo exchange, with its associated energy scale, the Kondo temperature T_K; (ii) the intra-impurity exchange splitting *J*. As we already mentioned, the Kondo exchange (9) gains energy by letting the impurity tunnel coherently among all available six configurations, but it is hampered by *J*, which instead tends to trap the impurity into a well-defined state.

If $J \gg T_K > 0$, the positive exchange splitting dominates and the impurity is essentially frozen into the lowest-energy spin-triplet configuration. The Kondo exchange projected onto the triplet subspace (4) is simply $H_K = J_K \vec{S}\cdot\vec{\mathcal{S}}$, describing a standard $S=1$ two-channel Kondo effect. This is known to be perfectly screened at low energy,[1,10] yielding a scattering phase shift $\delta = \pi/2$ in each spin and orbital channel.

In contrast, if $J \ll -T_K < 0$, the impurity gets trapped in the $S=0$, $T=1$, and $T^z=0$ configuration (5). Since Eq. (5) is non-degenerate, the Kondo exchange is ineffective, so that asymptotically the impurity decouples from the conduction bath. This implies a low-energy phase shift $\delta=0$. The main question that we try to address is how the model moves across the two limiting cases.

As it was pointed out in Ref. 8, this behavior is parallel to the two $S=1/2$ impurity Kondo model (2IKM) in the presence of a direct exchange between the impurity spins[2–4]. In that case, if the two spins are strongly ferromagnetically coupled, the model reduces to an $S=1$ two-channel Kondo model, while, if they are strongly antiferromagnetically coupled, the two spins bind together into a singlet and decouple from the conduction electrons, exactly as in our model. The two channels correspond in the 2IKM to the symmetric and antisymmetric combinations of the even and odd scattering channels with respect to the midpoint between the impurities. It was demonstrated in Ref. 4 that, provided a peculiar particle-hole symmetry holds, the non-Fermi-liquid unstable fixed point (UFP) found in Ref. 2 separates the Kondo-screened and unscreened regimes. In particular it was shown that while a particle-hole symmetry-breaking term

$$\delta H_{p\text{-}h} = -\,\mu_d \sum_{a\alpha} d^{\dagger}_{a\alpha} d_{a\alpha} - \sum_{\mathbf{k},a\alpha} \mu_{\mathbf{k}}\, c^{\dagger}_{\mathbf{k}a\alpha} c_{\mathbf{k}a\alpha}, \tag{11}$$

does not wash out the UFP, the latter is instead destabilized by the perturbation

$$\delta H_{rel} = -\,h_d \sum_{\alpha} d^{\dagger}_{1\alpha} d_{2\alpha} + \text{H.c.} - \sum_{\mathbf{k},\alpha} h_{\mathbf{k}}\, c^{\dagger}_{\mathbf{k}1\alpha} c_{\mathbf{k}2\alpha} + \text{H.c.} \tag{12}$$

Translated into our two-orbital language, the dangerous symmetry that needs to be preserved is just the $O(2)_{orbit}$ orbital symmetry. Therefore, unlike in the 2IKM, where the two scattering channels are generically not degenerate, in our case the instability towards $O(2)_{orbit}$ symmetry breaking does correspond to a physical instability. Hence, if orbital symmetry is unbroken, we do expect to find an UFP in our model, with similar properties as in the 2IKM. We notice that, in spite of the analogies, our model has a larger impurity Hilbert space than the 2IKM. In fact the $S=0$, $T=1$, and $T^z = \pm 1$ doublet of Eq. (6) is absent in the 2IKM, where it would correspond to doubly occupied impurities (the labels 1 and 2 for the *d* orbitals translate in the 2IKM into the two one-orbital impurities). Yet we can perturb our Hamiltonian by adding to *H* of Eq. (1) the term

$$H_G = G\, (T^z)^2, \tag{13}$$

with $G>0$, which raises the energy of the doublet. If $G \gg T_K$, the doublet effectively decouples from the low-energy sector, and our model should become equivalent to the 2IKM. In Sec. IV we show that indeed by increasing *G* our UFP smoothly transforms into the 2IKM one.

III. PHYSICAL REALIZATIONS

As we emphasized in the Introduction, our interest in model (1) plus eventually Eq. (13) is mainly motivated by its possible relevance for lattice models. In reality a formal correspondence between single-impurity and lattice models holds strictly only in the limit of large lattice coordination. Nevertheless we believe that this correspondence, at least close to a Mott transition, may remain valid even beyond that limit, making the single-impurity analysis of much broader interest. Therefore, although inversion of Hund's rules may indeed occur in realistic AIM's or in artificially designed quantum dot devices, here we rather focus on lattice models that map within DMFT into our AIM.

A. Two-band Hubbard model in the presence of an $e\otimes E$ Jahn-Teller coupling

Let us start by considering a two-band Hubbard model in which each site undergoes Jahn-Teller coupling to a doubly degenerate phonon. The Hamiltonian reads

$$H = -\frac{t}{\sqrt{z}}\sum_{a=1}^{2}\sum_{\sigma}\sum_{\langle ij\rangle}(c^{\dagger}_{ai\sigma}c_{aj\sigma}+\text{H.c.})+\frac{U}{2}\sum_{i}(n_i-2)^2 + 2J_H\sum_i[(T^x_i)^2+(T^y_i)^2]+\frac{\omega_0}{2}\sum_i\sum_{a=x,y}(q^2_{ia}+p^2_{ia}) - g\sum_i(q_{ix}\,T^x_i+q_{iy}\,T^y_i). \quad (14)$$

Here $-t/\sqrt{z}$ is the hopping matrix element between one site and its z neighbors and $J_H>0$ is a conventional Hund's exchange. q_{ix} and q_{iy} are the phonon coordinates at site i, p_{ix} and p_{iy} their conjugate momenta, ω_0 the phonon frequency, and g the Jahn-Teller coupling. The latter gives rise to a retarded electron-electron interaction whose Fourier transform is

$$g^2\sum_i\frac{\omega_0}{\omega^2-\omega_0^2}[T^x_i(\omega)T^x_i(-\omega)+T^y_i(\omega)T^y_i(-\omega)].$$

If the phonon frequency ω_0 is much larger than the quasiparticle bandwidth, we can safely neglect the ω dependence at low energy, so that the phonon-mediated interaction becomes unretarded and given by

$$-\frac{g^2}{\omega_0}\sum_i[(T^x_i)^2+(T^y_i)^2].$$

Within DMFT the Hamiltonian maps in the large-z limit onto the same AIM model as in Eq. (1) with

$$J = J_H-\frac{g^2}{2\omega_0}, \quad (15)$$

which may be either positive or negative. The case with $J<0$ as well as the starting model realistically including phonons has been recently studied by DMFT.[9,11]

B. Two-band Hubbard model with single-ion anisotropy

Another realization that may also be physically relevant is the following lattice model:

TABLE I. Mapping between the AIM interaction parameters and the two Hubbard plane parameters.

AIM	Two Hubbard planes
U	$\frac{1}{2}(U+V)-\frac{1}{8}J$
J	$-\frac{1}{4}J$
G	$U-V+\frac{1}{4}J$

$$H = -\frac{t}{\sqrt{z}}\sum_{a=1}^{2}\sum_{\sigma}\sum_{\langle ij\rangle}(c^{\dagger}_{ai\sigma}c_{aj\sigma}+\text{H.c.})+\frac{U}{2}\sum_i(n_i-2)^2 - 2J_H\sum_i\vec{S}_i\cdot\vec{S}_i+D\sum_i(S^z_i)^2. \quad (16)$$

For $J_H>0$ and $D\neq 0$ this model describes a two-band Hubbard model with conventional Hund's rules, favoring a spin-triplet two-electron configuration, in the presence of a single-ion anisotropy that splits the spin triplet into a singlet with $S^z=0$ and a doublet with $S^z=\pm 1$. If $D>0$, the $S^z=0$ configuration is favored. Upon interchanging $\vec{S}\leftrightarrow\vec{T}$, this model maps in the $z\to\infty$ limit onto Eq. (1) with

$$J=-J_H, \quad G=D-2J_H. \quad (17)$$

C. Two coupled Hubbard planes

Finally let us consider two coupled single-band Hubbard planes described by the Hamiltonian

$$H = -\frac{t}{\sqrt{z}}\sum_{a=1}^{2}\sum_{\sigma}\sum_{\langle ij\rangle}(c^{\dagger}_{ai\sigma}c_{aj\sigma}+\text{H.c.})+\frac{U}{2}\sum_{a,i}(n_{ai}-1)^2 + \sum_i J\vec{S}_{1i}\cdot\vec{S}_{2i}+V(n_{1i}-1)(n_{2i}-1), \quad (18)$$

where $a=1,2$ labels the two planes and $-t/\sqrt{z}$ is the in-plane hopping between one site and its z neighbors. In the limit $z\to\infty$, this model maps by DMFT onto an AIM self-consistently coupled to a bath.[5] The relations between the interaction parameters of the AIM, Eq. (1) plus Eq. (13), and those of Eq. (18) are given in Table I.

In reality it is more interesting to consider the model (18) with $J=V=0$ but in the presence of an interplane hopping

$$-t_{\perp}\sum_{i\sigma}(c^{\dagger}_{1i\sigma}c_{2i\sigma}+\text{H.c.}). \quad (19)$$

In the limit of large lattice coordination, this model maps close to the MIT onto a two-orbital AIM with an hybridization width at the chemical potential much smaller than U. Since by Table I $G=U$, we can safely project out of the low-energy subspace the doublet (6). The effective AIM within the impurity subspace that includes the singlet (5) and the spin triplet is

$$H_{AIM} = H_c+J_K(\vec{S}_1+\vec{S}_2)\cdot\vec{\mathcal{S}}+J\,\vec{S}_1\cdot\vec{S}_2+J_K\frac{t_{\perp}}{U}\mathcal{T}^x, \quad (20)$$

where H_c and J_K have been defined in Eqs. (1) and (10), $\vec{S}_1$ and $\vec{S}_2$ are the impurity spin operators for the singly occupied

orbitals 1 and 2, while $\vec{S}$ and T^x are, respectively, the conduction-electron spin-density operator and x component of the pseudospin density operator, $\vec{T}$, at the impurity site. The impurity antiferromagnetic exchange, $J=4t_\perp^2/U$, lowers the energy of the singlet (5) with respect to the spin triplet. Therefore J alone might induce an UFP within the phase diagram, just like in our model as well as in the 2IKM. However $t_\perp$ also introduces a T^x scattering potential at the impurity site, the last term on the right-hand side of Eq. (20), which is known to be relevant at the UFP. In this respect $t_\perp$ plays an intriguing role: on one hand it provides a mechanism, the antiferromagnetic exchange J, able to stabilize a nontrivial fixed point, but, in the meantime, it also prevents the fixed point from being reachable. Yet we might wonder whether the critical region around the UFP is completely or only partially washed out. In the latter case we should expect that the physics of the lattice model close to the MIT is still influenced by the UFP, with interesting consequences. We will come back to this issue in Sec. VII.

IV. NUMERICAL RENORMALIZATION GROUP RESULTS

To study the AIM (1) we used the Wilson numerical renormalization group (NRG) method.[12] This technique is known to provide a detailed description of the low-energy behavior, thus allowing a faithful characterization of the fixed points as well as of their stability domain. In addition, dynamical properties are also accessible by NRG, which, as we are going to show, are of notable interest.

Within NRG the conduction band is logarithmically discretized and mapped onto a one-dimensional chain with nearest neighbor hopping integrals that decrease exponentially along the chain. The Hamiltonian of a chain with $N+1$ sites is defined by

$$H_N=\Lambda^{(N-1)/2}\Bigg\{\sum_{n=0}^{N-1}\Lambda^{-n/2}\xi_n(c_{na\alpha}^\dagger c_{(n+1)a\alpha}+c_{(n+1)a\alpha}^\dagger c_{na\alpha})+\tilde{\Delta}_0^{1/2}(c_{0a\alpha}^\dagger d_{a\alpha}+d_{a\alpha}^\dagger c_{0a\alpha})+\frac{\tilde{U}}{2}(n_d-2)^2+2\tilde{J}[(T^x)^2+(T^y)^2]\Bigg\}. \tag{21}$$

Here $\tilde{U}=C_\Lambda U$, $\tilde{J}=C_\Lambda J$, $\tilde{\Delta}_0=C_\Lambda^2(2\Delta_0/\pi)$, [see Eq. (7)], where $C_\Lambda=(2\Lambda/1+\Lambda)$ and all energies are measured in units of half the conduction bandwidth. The rescaling factor $\Lambda^{(N-1)/2}$ at the beginning of Eq. (21) keeps the lowest-energy scale in H_N of order one at each iteration. The original Hamiltonian is recovered in the limit of infinite chain length:

$$H=\lim_{N\to\infty}C_\Lambda^{-1}\Lambda^{-(N-1)/2}H_N. \tag{22}$$

The size N of the chain determines the infrared cutoff, e.g., the temperature T, on a logarithmic scale ($T\sim\Lambda^{-N/2}$). The method essentially consists of diagonalizing the model on a finite size chain, e.g., N, and iteratively increasing the size by one site, from N to $N+1$, keeping only the low-energy part of the N-site spectrum. (In our calculations we typically kept up to the lowest 2000 states, not counting degeneracies, and used Λ between 2 and 3. We did check that these numbers are sufficient to get accurate results.)

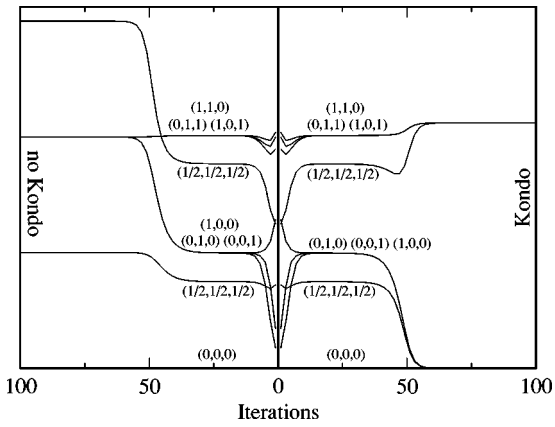

FIG. 1. Lowest-energy levels versus the chain size N. The right/left panels correspond to a deviation $\delta J/J^*=\pm 4\cdot 10^{-3}$ from the fixed point value J^*. The levels are labeled by the quantum numbers (Q,T^z,S), where Q is one-half of the added charge with respect to the ground-state value.

We restrict our analysis to large values of U, where valence fluctuations on the impurity are substantially suppressed. Here, as we discussed, the AIM effectively behaves like the Kondo model (8). We fix both U and Δ and span the phase space by varying the exchange parameter J.

A. Low-energy spectrum at the fixed points

First of all we identify the fixed points by analyzing the low-energy spectra (with N typically up to one hundred). Since the conventional size dependence of the level spacing is absorbed by the factor $\Lambda^{(N-1)/2}$ in Eq. (21), the low-lying energy levels flow to constant values whenever the model is close to a fixed point. Figure 1 shows that there are two different asymptotic regimes separated by a critical value $J^*<0$. In order to facilitate the interpretation of that figure, we recall that the ground state of a particle-hole symmetric free chain with $N+1$ sites is unique if N is odd and degenerate if N is even.

For $J>J^*$ the low-energy spectrum of a chain with *odd* number, $N+1$, of sites flows towards that of a free chain with an *even* number of sites and vice versa. This is evident in the right panel of Fig. 1 where the ground state of the chain with odd N becomes asymptotically degenerate as for a chain with even N. Apart from the ground-state degeneracy, also the low-lying spectrum, i.e., degeneracy and quantum numbers of the levels as well as the level spacings, coincides with that of a free chain. As usual, this is as if the first site of the chain were locked to form a spin and orbital singlet configuration with the impurity, hence becoming unaccessible to the conduction electrons that thus acquire a $\pi/2$ phase shift per conduction channel. It is a conventional Kondo-screened phase.

For $J<J^*$ the situation is reversed: the low-energy spectrum of an odd (even) chain flows to that of an odd (even)

free chain. Indeed, as shown in the left panel of Fig. 1, the ground state with N odd remains nondegenerate for large N. This case corresponds to an unscreened phase with the impurity asymptotically decoupled from the conduction bath. The phase shift is consequently $\delta=0$.

Between the Kondo screened and unscreened phases we do find a nontrivial fixed point, as is visible in the intermediate crossover region of the spectrum (see Fig. 1.) The peculiar non-Fermi-liquid character of this intermediate coupling UFP is evident by the nonuniform spacing of the low-energy levels. A careful analysis of the UFP spectrum reveals that it is just the same as that found in the particle-hole-symmetric 2IKM.[4] In Table II we compare the energies E of the lowest-lying levels of the Wilson chain at the UFP, as obtained by NRG, with the prediction x of conformal field theory for the 2IKM.[4] The agreement is proof that the UFP is indeed the same in both models.

B. Impurity properties at the UFP

Additional information are provided by the average values of the impurity spin, $\langle\vec{S}\cdot\vec{S}\rangle$, pseudospin, $\langle\vec{T}\cdot\vec{T}\rangle$, and its z component, $\langle(T^z)^2\rangle$. By symmetry, the impurity density matrix is diagonal in the six two-electron configurations. The diagonal elements represent the occupation probabilities $P(S,S^z,T,T^z)$ of states with quantum numbers S, S^z, T and T^z. In the large-U limit, where impurity configurations with $n\neq 2$ have negligible weight, we can write

$$P(0,0,1,0)=\cos^2\theta,$$

$$P(0,0,1,+1)=P(0,0,1,-1)=\frac{1}{2}\sin^2\theta\,\sin^2\phi,$$

$$P(1,+1,0,0)=P(1,0,0,0)=P(1,-1,0,0)=\frac{1}{3}\sin^2\theta\,\cos^2\phi, \tag{23}$$

from which we derive

$$\langle\vec{S}\cdot\vec{S}\rangle=2\,\sin^2\theta\,\cos^2\phi,$$

$$\langle\vec{T}\cdot\vec{T}\rangle=2(\cos^2\theta+\sin^2\theta\,\sin^2\phi),$$

$$\langle(T^z)^2\rangle=\sin^2\theta\,\sin^2\phi. \tag{24}$$

In Fig. 2 we plot the angles θ and ϕ as obtained through Eqs. (24) by the numerically calculated average values. The UFP is characterized by $\theta=\phi=\pi/4$, namely, by the value 1/2 of the occupation probability of the singlet state (5). The precise value of the other occupation probabilities, in other words, of ϕ, are instead not relevant, apart from the obvious fact that their sum should be 1/2 too. In fact, if we add the term (13) with $G>0$, we do find the same UFP, the locations of which now depends also on G, which is still identified by $P(0,0,1,0)=1/2$, i.e. $\theta=\pi/4$, although the weight of the spin triplet is enhanced with respect to the doublet (6), $\phi<\pi/4$. For large G we do recover the 2IKM values $\theta=\pi/4$ and $\phi=0$ (see Fig. 3).

TABLE II. Energies E of the low-energy levels and their degeneracy (*Deg.*) at the unstable fixed point. The levels are labeled by the quantum numbers Q, half of the deviation of the number of electrons with respect to the ground state, S, total spin, and T^z, total z component of the pseudospin. The value x is the prediction of conformal field theory for the two-impurity Kondo model (Ref. 4). Notice the anomaly of the member within the $(1/2,1/2,1/2)$ multiplets identified by an asterisk, which was also found in Ref. 4. There an explanation for the discrepancy was proposed.

Q	T^z	S	x	E	Deg.
0	0	0	0	0.00000	1
$\frac{1}{2}$	$\frac{1}{2}$	$\frac{1}{2}$	$\frac{3}{8}$	0.37260	8
0	0	1	$\frac{1}{2}$	0.49615	3
0	1	0	$\frac{1}{2}$	0.49583	2
1	0	0	$\frac{1}{2}$	0.49631	2
$\frac{1}{2}$	$\frac{1}{2}$	$\frac{1}{2}$	$\frac{7}{8}$	0.88021	8
0	0	0	1	0.99714	1
				1.00216	1
				1.00311	1
0	0	1	1	1.00279	3
0	1	1	1	1.00248	6
1	0	1	1	1.00295	6
1	1	0	1	1.00264	4
$\frac{1}{2}$	$\frac{1}{2}$	$\frac{1}{2}$	$1+\frac{3}{8}$	1.38880	8
				1.38945	8
				1.51556*	8
$\frac{1}{2}$	$\frac{1}{2}$	$\frac{3}{2}$	$1+\frac{3}{8}$	1.38924	16
$\frac{1}{2}$	$\frac{3}{2}$	$\frac{1}{2}$	$1+\frac{3}{8}$	1.38859	8
$\frac{3}{2}$	$\frac{1}{2}$	$\frac{1}{2}$	$1+\frac{3}{8}$	1.38957	8
0	0	0	$1+\frac{1}{2}$	1.55944	1
0	0	1	$1+\frac{1}{2}$	1.50195	3
				1.55863	3
				1.55983	3
				1.60582	3
0	1	0	$1+\frac{1}{2}$	1.50141	2
				1.55943	2
				1.60467	2
0	1	1	$1+\frac{1}{2}$	1.55904	6
1	0	0	$1+\frac{1}{2}$	1.50222	2
				1.55883	2
				1.60636	2
1	0	1	$1+\frac{1}{2}$	1.55964	6
1	1	1	$1+\frac{1}{2}$	1.55923	12

C. Approach to the fixed points

As we said the low-energy spectrum both in the Kondo-screened and unscreened phases flows to that of a free chain, with one less site in the former case. The flow towards the asymptotic spectrum can be described by a free chain in the presence of a local perturbation term[12] acting on the first available site, denoted as site 0, of the conduction chain, which is actually the second site in the Kondo-screened

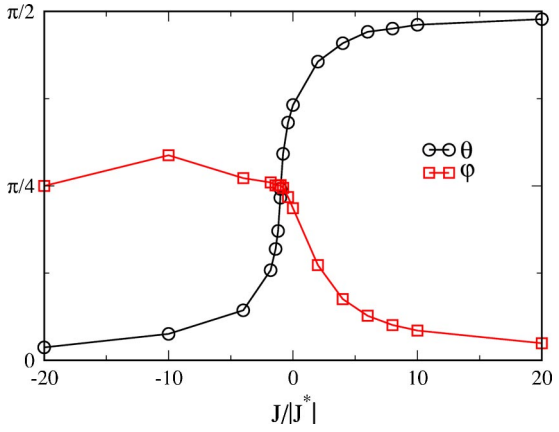

FIG. 2. (Color online) The angles θ and ϕ as defined through Eq. (24). Notice that the fixed point is identified by $\theta=\phi=\pi/4$.

phase. By symmetry considerations this local term can be in general written as

$$\delta H_* = -t_* \sum_{a\alpha} (c^\dagger_{0a\alpha} c_{1a\alpha} + \text{H.c.}) + \frac{U_*}{2}(n_0-2)^2 + J_{S*}\vec{\mathcal{S}}_0 \cdot \vec{\mathcal{S}}_0 + J_{T*}\vec{\mathcal{T}}_0 \cdot \vec{\mathcal{T}}_0 - 2(J_{S*}+J_{T*})(\mathcal{T}^z_0)^2. \quad (25)$$

We choose this particular form because it has the advantage that the energy of the center of gravity of each multiplet with given charge n_0 is just $U_*(n_0-2)^2/2$. Upon approaching the UFP on both sides, we find that $U_* \sim J_{S*}=\gamma \to +\infty$, $J_{T*} \sim -5\gamma \to -\infty$, and $t_* \sim 3\gamma/8 \to +\infty$. The behavior of t_* implies a divergence of the impurity contribution to the specific heat coefficient. Namely, if δC_V is the variation of the specific heat with respect to its value C_V in the absence of the impurity, then

$$\frac{\delta C_V}{C_V} \sim \rho_c\, t_* \to \infty.$$

In reality, it is more convenient to analyze the NRG results by invoking the Fermi-liquid theory, which we present

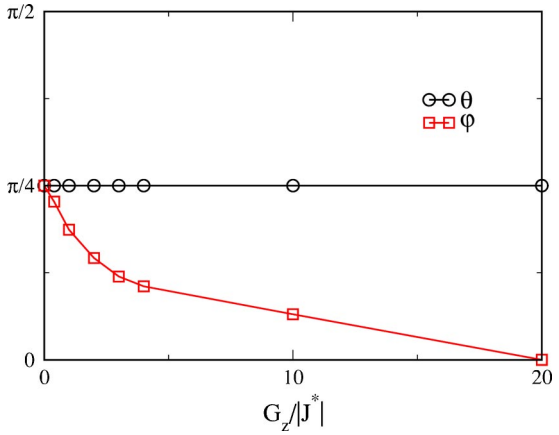

FIG. 3. (Color online) The UFP values of θ and ϕ along the path parametrized by the coupling G from our model to the 2IKM model.

in the Appendix. Through NRG, one can calculate the Wilson ratios related to the conserved quantities,[12] namely, the total charge, spin, and z component of $\vec{T}$. If $\delta\chi_i$ is the variation of the susceptibility with respect to the value χ_i without the impurity, where $\chi_i=\chi_C,\chi_S,$and $\chi^{\|}_T$ are the charge, spin, and T^z susceptibilities, then the Wilson ratios R_i are defined through

$$R_i = \frac{\delta\chi_i}{\chi_i}\frac{C_V}{\delta C_V}.$$

On the other hand, Fermi-liquid theory implies also that

$$R_i = 1 - A_i, \quad (26)$$

where A_i is the dimensionless quasiparticle scattering amplitude in channel i defined in Eq. (A11) through the scattering vertex at low incoming and outgoing frequencies and the quasiparticle density of states at the chemical potential, [see Eq. (A8)]. In general, we can introduce a scattering amplitude for each particle-hole and particle-particle channel. In particular, besides A_C, A_S, and $A^{\|}_T$, we consider the particle-hole scattering amplitudes in the T^x channel, which is degenerate with the T^y channel, $A^{\perp}_T$, as well as in the spin orbital channels $\vec{S}T^z$, $A^{\|}_{ST}$, and $\vec{S}T^{x(y)}$, $A^{\perp}_{ST}$. In addition we introduce the amplitudes in the particle-particle channels, namely $\mathcal{A}^1$ in the spin-triplet orbital-singlet Cooper channel and $\mathcal{A}^0_0$ and $\mathcal{A}^0_{\pm}$ in the spin-singlet orbital-triplet channels with $T^z=0$ and $T^z=\pm 1$, respectively. As shown in the Appendix, all particle-hole scattering amplitudes can be expressed through the particle-particle amplitudes:

$$A_C = \frac{1}{4}(6\mathcal{A}^1 + 2\mathcal{A}^0_0 + 4\mathcal{A}^0_{\pm}), \quad (27)$$

$$A_S = \frac{1}{4}(2\mathcal{A}^1 - 2\mathcal{A}^0_0 - 4\mathcal{A}^0_{\pm}), \quad (28)$$

$$A^{\|}_T = \frac{1}{4}(-6\mathcal{A}^1 - 2\mathcal{A}^0_0 + 4\mathcal{A}^0_{\pm}), \quad (29)$$

$$A^{\perp}_T = \frac{1}{4}(-6\mathcal{A}^1 + 2\mathcal{A}^0_0), \quad (30)$$

$$A^{\|}_{ST} = \frac{1}{4}(-2\mathcal{A}^1 + 2\mathcal{A}^0_0 - 4\mathcal{A}^0_{\pm}), \quad (31)$$

$$A^{\perp}_{ST} = \frac{1}{4}(-2\mathcal{A}^1 - 2\mathcal{A}^0_0). \quad (32)$$

Since we are able to calculate by NRG the three Wilson ratios R_C, which is zero in the Kondo limit, R_S, and $R^{\|}_T$, we can also determine the three unknown particle-particle scattering amplitudes through Eqs. (26)–(29), which we plot in Fig. 4.

The first thing to notice is that approaching the UFP,

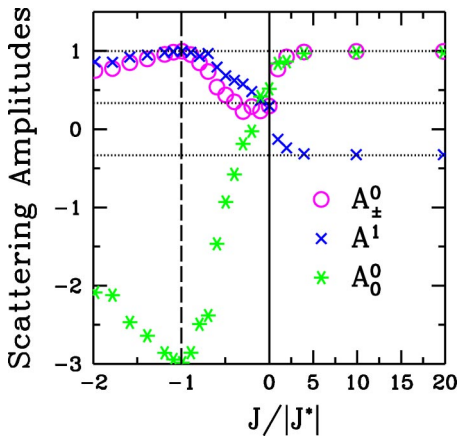

FIG. 4. (Color online) The scattering amplitudes in the various particle-particle channels as a function of J measured in units of the UFP J^*. Notice the agreement with the values predicted by general arguments presented in the Appendix at the UFP, $J/|J^*|=-1$, at the SU(4) point, $J/|J^*|=0$, and in the limit of the $S=1$ two-channel Kondo model, $J/|J^*|\gg 1$.

$$\mathcal{A}_0^0 \simeq A_T^{\perp} \simeq A_{ST}^{\parallel} \simeq -3,$$

while all the other A_i's tend to 1, implying vanishing Wilson ratios. The fixed point seems therefore to display a large hidden symmetry, actually a SO(7) as identified by Ref. 4. The UFP is equally unstable in the s-wave Cooper channel with $S=0$, $T=1$, and $T^z=0$, as well as in the particle-hole $T^{x(y)}$ and $\vec{S}T^z$ channels.[8,13] All of them correspond to physical instabilities as we anticipated, unlike what happens in the 2IKM. In contrast any external field in the other channels do not spoil the UFP, in particular, in the charge, spin, and T^z particle-hole channels, which refer to conserved quantities.

The physics around and right at the UFP has been revealed by conformal field theory and bosonization.[3,4,8,14,15] Due to the existence of two energy scales, the Kondo temperature T_K and the exchange splitting J, the quenching of the impurity degrees of freedom takes place in two steps. First, around an energy scale $T_+ \sim \max(T_K, |J|)$, most of the ln 6 entropy of the two-electron impurity multiplets is removed, leaving behind a residual entropy $\ln\sqrt{2}$, which gets quenched only below a lower energy scale $T_- \sim 1/\gamma$. The latter depends quadratically upon the deviation from the UFP, namely $T_- \sim |J-J^*|^2/T_+$. The entropy has a low energy linear behavior, $S(T) \sim T/T_-$, followed above T_- by another linear one, $S(T) - \ln\sqrt{2} \sim T/T_+$.[4,15] At the fixed point, $T_-=0$, there is a finite residual entropy $S(0)=\ln\sqrt{2}$ and $S(T)-S(0) \sim T/T_+$. A perturbation in any of the relevant channels washes out the fixed point, cutting off the infrared singularities close to the UFP on an energy scale that depends quadratically upon the strength of the perturbation. In Sec. VII we analyse more explicitly the stability or instability of the UFP towards symmetry-breaking fields in particle-hole channels.

D. Influences of the single-impurity behavior in a DMFT calculation

Let us now instead discuss the above results in connection with DMFT. Suppose there is a lattice model that maps in the limit of large lattice coordination onto the AIM (1) with $J<0$. If the model is driven towards a Mott metal-insulator transition, the effective AIM is necessarily pushed into a regime in which $T_K \sim |J|$, namely, in the critical region around the UFP. As shown in Fig. 4, the s-wave scattering amplitude $\mathcal{A}_0^0$ as well as the equally relevant $A_T^{\perp}$ and $A_{ST}^{\parallel}$ are strongly attractive in an entire interval around the UFP. This suggests that the impurity fixed-point instability might transform by DMFT self-consistency into a whole pocket where the model generates spontaneously a bulk symmetry-breaking order parameter along one of the relevant channels. As we argued in Ref. 8, if nesting or Van Hove singularities are absent, it is most probable that the dominant instability will occur in the Cooper channel, the only one which is singular in any dimensions and for any band structure with a finite quasiparticle density of states at the chemical potential. This has been indeed confirmed by very recent DMFT calculations in Refs. 9 and 11.

The other interesting observation is that in the conventional Hund's regime, the Kondo-screened phase with $J>0$, an attraction in the spin-triplet $T=0$ channel develops, $\mathcal{A}^1<0$. In realistic lattice models that map onto the AIM with $J>0$ in the limit of large lattice coordination, spin-triplet superconductivity would compete with bulk magnetism. Yet, if magnetism is frustrated, spin-triplet superconductivity might emerge. In particular, since increasing the Hubbard U in the lattice model implies decreasing T_K in the AIM, which is the same as increasing the effective strength of $J>0$, we should expect that spin-triplet superconductivity is enhanced near the MIT. This has been recently observed by DMFT.[11] However, the enhancement of the spin-triplet amplitude is not as dramatic as for the spin-singlet amplitude near the UFP at $J<0$. This situation would change in the presence of a single-ion anisotropy that favors, e.g., spin-triplet pairing with $S^z=0$ [see the model, Eq. (16)]. As we showed, this model is equivalent to Eq. (1) upon interchanging the role of $\vec{T}$ with $\vec{S}$. This suggests that the lattice model that maps by DMFT onto Eq. (16) with $D>0$ would still enter a local critical regime before the MIT. Here the tendency towards spontaneous generation of a bulk order parameter should be dramatically enhanced in the particle-hole channels S^x, S^y, and $\vec{T}S^z$ as well as in the spin-triplet Cooper channel with $S^z=0$: $c_{1\uparrow}^{\dagger}\, c_{2\downarrow}^{\dagger} - c_{2\uparrow}^{\dagger}\, c_{1\downarrow}^{\dagger}$.

V. IMPURITY SPECTRAL FUNCTION

The impurity DOS, $\rho(\epsilon)$, is defined through

$$\rho(\epsilon) = -\frac{1}{2\pi}\lim_{\eta\to 0}[G(\epsilon + i\eta) - G(\epsilon - i\eta)], \tag{33}$$

where $G(i\epsilon_n)$ is the impurity Green's function in Matsubara frequencies, which, by symmetry, is diagonal in spin and orbital indices, and independent of them. In general,

$$G(i\epsilon_n)^{-1} = i\epsilon_n - \Delta(i\epsilon_n) - \Sigma(i\epsilon_n) = G_0(i\epsilon_n)^{-1} - \Sigma(i\epsilon_n), \tag{34}$$

where $G_0(i\epsilon_n)$ is the noninteracting, $U=J=0$, Green's function,

$$\Delta(i\epsilon_n) = V_d^2 \sum_{\mathbf{k}} \frac{1}{i\epsilon_n - \epsilon_{\mathbf{k}}} \tag{35}$$

is the hybridization function, and $\Sigma(i\epsilon_n)$ the impurity self-energy. Let us follow the behavior of the DOS as the interaction is switched on. We will imagine increasing slowly both U and $|J|$ at fixed $U/|J| \gg 1$ with $J<0$. When U is small, one can show by perturbation theory that

$$\mathrm{Im}\,\Sigma(\epsilon) \sim \epsilon^2,$$

which is the standard result that the quasiparticle decay rate vanishes faster than the frequency. Therefore at the chemical potential, $\epsilon=0$, the impurity DOS is not affected by a weak interaction, since

$$\rho(0) = -\frac{1}{\pi} \lim_{\eta\to 0} \mathrm{Im}\; G(0+i\eta) = -\frac{1}{\pi} \lim_{\eta\to 0} \mathrm{Im}\; G_0(0+i\eta)$$

$$= \frac{1}{\pi\Delta_0} = \rho_0, \tag{36}$$

where $\Delta_0 = -\mathrm{Im}\,\Delta(0+i\eta)$ was introduced in Eq. (7), and ρ_0 denotes the noninteracting DOS at the chemical potential. In a single-orbital AIM, the above result remains valid even when the interaction is very large. In our case we may expect that something nontrivial should instead occur. Indeed, upon increasing U, the AIM enters the Kondo regime, with a Kondo temperature exponentially decreasing with U. Therefore at some critical U_c, when $T_K \sim |J|$, the AIM has to cross the non-Fermi-liquid UFP. Namely the UFP of our AIM can also be attained by increasing the interaction strength, signaling a breakdown of the conventional perturbation theory. We now discuss how this criticality shows up in the spectral properties.

The impurity DOS can be obtained by NRG by directly evaluating the spectral function

$$A_{a\alpha}(\omega) = \frac{1}{Z}\sum_{m,n} |\langle m|d_{a\alpha}^\dagger|n\rangle|^2 \delta(\omega - (E_n - E_m))(e^{-\beta E_n} + e^{-\beta E_m}). \tag{37}$$

For any finite chain $A(\omega)$ is a discrete sum of δ peaks. A smooth DOS is obtained by broadening the peaks, which we do following Ref. 16 through the transformation

$$\delta(\omega - \omega_{nm}) \to \frac{e^{-b^2/4}}{b\;\omega_{nm}\sqrt{\pi}} \exp\left[-\frac{(\ln\,\omega - \ln\,\omega_{nm})^2}{b^2}\right], \tag{38}$$

where $\omega_{nm} = E_n - E_m$ and $b=0.55$ for $\Lambda=2$.

In Fig. 5 we show the outcome of the numerical calculation. On the Kondo-screened side of the UFP, the DOS shows a narrow Kondo-resonance on top of a broader one. The height at the chemical potential is $\rho(0)=\rho_0$, as expected in a Kondo-screened phase. In contrast, in the unscreened side of the UFP, the narrow peak transforms into a narrow pseudogap within the broad resonance. Numerically we find that $\rho(\epsilon) \sim \epsilon^2$. As discussed before, this implies that the conventional behavior $\mathrm{Im}\,\Sigma(\epsilon) \sim \epsilon^2$ breaks down across the UFP. Exactly at the fixed point, both the narrow peak and the pseudogap disappear, leaving aside only the broad resonance. The calculated DOS at the chemical potential seems to be half of its noninteracting value (see Fig. 5). In other words, our numerical results point to a DOS at the chemical potential that jumps across the UFP, being $\rho(0)=\rho_0$ everywhere in the Kondo-screened phase, $\rho(0)=0$ in the unscreened one, and $\rho(0)=\rho_0/2$ right at the UFP.

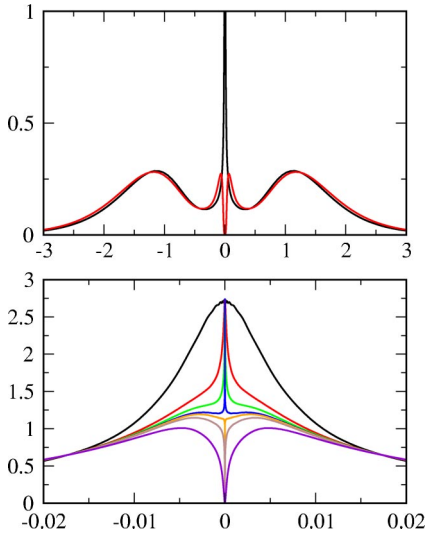

FIG. 5. (Color online) Impurity DOS in the presence of particle-hole symmetry across the fixed point. The temperature is set by the length of the chain; it is practically zero. In the upper panel we draw the DOS's well inside the Kondo screened phase ($J/J^*=0$) and the unscreened phase ($J/J^*=5.75$). Here $U=2$, $\Delta_0 = U/(6\pi)$, and J_* turns out to be $\simeq -0.0035$, all in units of half the conduction bandwidth. Notice the narrow peak, which transforms into a narrow pseudogap. In the lower panel we show in more detail the behavior of the low-energy DOS across the UFP. (From top to bottom, $J/J^* = 0, 0.859, 0.945, 0.988, 1.002, 1.031, 1.146$.)

VI. MODELING THE IMPURITY DENSITY OF STATES

It is possible to infer an analytical expression of the impurity DOS. First of all we notice that the values at the chemical potential in the screened and in the unscreened Kondo regimes are compatible with general scattering theory. In both phases the impurity has disappeared at low energy, either because it has been absorbed by the conduction sea or because J has taken care of quenching the impurity spin and orbital degrees of freedom. This in turns means that what remains at low energy is just a potential scattering experienced by the conduction electrons plus a local electron-electron interaction term. The on-shell S-matrix at the chemical potential has, in general, elastic and inelastic contributions (see Ref. 17). At zero temperature only the former survives. Since we considered just s-wave scattering, the elastic component of the S matrix is given by

$$S(0) = 1 - 2\pi i \rho_c T(0) = 1 - 2\pi\Delta_0\rho(0), \tag{39}$$

where ρ_c is the conduction electron DOS at the chemical potential per spin and band, and the T matrix is defined through the conduction electron Green's function $\mathcal{G}$ by

$$\mathcal{G} = \mathcal{G}_0 + \mathcal{G}_0\, T\, \mathcal{G}_0.$$

On the other hand, the S matrix is related to the scattering phase shift by

$$S(0) = e^{2i\delta(0)}. \tag{40}$$

In the Kondo-screened phase, we know that $\delta(0)=\pi/2$, which, through Eqs. (40) and (39), implies $\rho(0)=1/\pi\Delta_0$, namely its noninteracting value ρ_0. On the other hand, in the unscreened regime $\delta(0)=0$ and hence $\rho(0)=0$, as we indeed find. It has been proposed that at the non-Fermi-liquid fixed point of the overscreened $S=1/2$ two-channel Kondo model the S matrix is instead purely inelastic[3,18,19]. That would imply a vanishing elastic contribution, $S(0)=0$ in Eq. (39), and in turn a DOS at the UFP,

$$\rho(0) = \frac{1}{2\pi\Delta_0} = \frac{1}{2}\rho_0, \tag{41}$$

which is indeed compatible with our numerical results.[20] Yet there is a difference between the UFP of our model, equivalently of the 2IKM, and the non-Fermi-liquid fixed point of the $S=1/2$ two-channel Kondo model. While in the latter the specific heat has a singular temperature behavior right at the UFP, in our model it has a conventional linear behavior. The above observation suggests the following simple analytical expression of the low-energy impurity DOS:

$$\rho_\pm(\epsilon) = \frac{\rho_0}{2}\left(\frac{T_+^2}{\epsilon^2+T_+^2} \pm \frac{T_-^2}{\epsilon^2+T_-^2}\right), \tag{42}$$

where the plus sign refers to the Kondo-screened phase and the minus to the unscreened one. The two energy scales have the same meaning as in the preceding section. In particular, T_- controls the deviations from the UFP, so that right at the UFP, when $T_-=0$, the DOS is

$$\rho_*(\epsilon) = \frac{\rho_0}{2}\frac{T_+^2}{\epsilon^2+T_+^2}. \tag{43}$$

The model DOS (42) also implies a model impurity Green's function in Matsubara frequencies:

$$G_\pm(i\epsilon_n) = \frac{1}{2\Delta_0}\left(\frac{T_+}{i\epsilon_n + iT_+\ \mathrm{sgn}\epsilon_n} \pm \frac{T_-}{i\epsilon_n + iT_-\ \mathrm{sgn}\epsilon_n}\right). \tag{44}$$

The fixed point Green's function, $G_*(i\epsilon_n)$, is identified by $T_-=0$. The impurity self-energy can then be extracted by the relation

$$\Sigma_\pm(i\epsilon_n) = i\epsilon_n + i\Delta_0\ \mathrm{sgn}\ \epsilon_n - G_\pm(i\epsilon_n)^{-1}.$$

In particular, at low frequency we find that

$$i\epsilon_n - \Sigma_+(i\epsilon_n) \simeq i\epsilon_n\frac{\Delta_0}{2}\left(\frac{1}{T_+}+\frac{1}{T_-}\right), \tag{45}$$

in the Kondo-screened phase, hence a standard linear behavior. In contrast, in the unscreened regime the self-energy is singular:

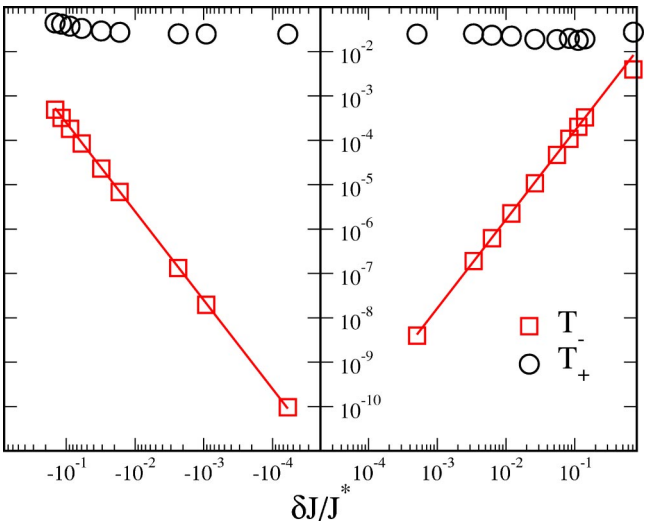

FIG. 6. (Color online) Fit values of T_+ and T_- close to the UFP. The lines are quadratic fits, $T_-=A(\delta J)^2$. The Hamiltonian parameters have the same values as in Fig. 5.

$$i\epsilon_n - \Sigma_-(i\epsilon_n) \simeq -\frac{1}{i\epsilon_n}\frac{2\Delta_0 T_+ T_-}{T_+ - T_-}. \tag{46}$$

Finally, at the fixed point the self-energy is finite at zero frequency, being given by

$$i\epsilon_n - \Sigma_*(i\epsilon_n) = i\Delta_0\frac{T_+ + 2\epsilon_n}{T_+}. \tag{47}$$

We have checked that the model self-energy gives indeed a good representation of the actual numerical results. In Fig. 6 we draw the fit values of T_+ and T_- around the UFP.

We can further test the consistency of the approach by invoking the scattering theory, which, by Friedel's sum rule, allows us to identify the scattering phase shifts through

$$\delta(\epsilon) = \mathrm{Im}\ \ln\ G(\epsilon + i0^+). \tag{48}$$

By means of our ansatz for the impurity Green's function (44) we readily find that the expression of the low-energy phase shifts is

$$\delta_+(\epsilon) \simeq \frac{\pi}{2} + \frac{\epsilon}{2}\left(\frac{1}{T_+}+\frac{1}{T_-}\right) \equiv \frac{\pi}{2} + \alpha_+\epsilon \tag{49}$$

within the Kondo-screened regime, and

$$\delta_-(\epsilon) \simeq \epsilon\left(\frac{1}{T_+}+\frac{1}{T_-}\right) \equiv \alpha_-\epsilon, \tag{50}$$

in the pseudogap unscreened phase, consistent with our starting assumption. Moreover, by the energy dependence of the phase shifts, we can calculate the impurity correction to the specific heat:

$$\frac{\delta C_V}{C_V} = \frac{\alpha_\pm}{\pi\rho_c}. \tag{51}$$

VII. PARTICLE-HOLE SYMMETRY-BREAKING TERMS

In this section we analyze more in detail various symmetry-breaking terms in the particle-hole channel. In particular we are going to consider the three following perturbations to the original Hamiltonian (1) with $\nu=0$:

$$\delta H_{p-h} = \nu\, U\, n_d \equiv \frac{h_{p-h}}{2} n_d, \tag{52}$$

$$\delta H_z = h_z\, T^z, \tag{53}$$

$$\delta H_x = h_x\, T^x. \tag{54}$$

The term (52) breaks particle-hole symmetry trying to occupy the impurity with $2-\nu$ electrons instead of two [see Eq. (1)]. The other terms (53) and (54) split the orbital degeneracy. It is convenient to decompose the orbital O(2) symmetry into the continuous U(1) symmetry related to proper rotations around the z axis, and a discrete Z_2, corresponding to interchanging the two orbitals. Then δH_z breaks the orbital Z_2 while δH_x breaks the orbital U(1). Among them, only the latter, δH_x, is predicted to be relevant and wash out the fixed point, at least according to bosonization.[8] Actually this looks a bit strange if one invokes naively the argument of Ref. 4 to demonstrate the existence of an UFP in the absence of any particle-hole symmetry-breaking term. This argument is based on the observation that, when $O(2)_{orbit}$ symmetry holds, the phase shifts in both orbital channels have to be equal, $\delta_1=\delta_2$. By general particle-hole symmetry, this further implies that $2\delta_1=2\delta_2=0 \bmod(\pi)$. Since for $J\gg T_K>0$ we know that $\delta_1=\delta_2=\pi/2$, while for $J\ll -T_K<0$, $\delta_1=\delta_2=0$, there must necessarily be a fixed point in between.

Let us assume now that the T^z term (53) is present and follow Ref. 4 to demonstrate that the necessary condition for the existence of an intermediate fixed point does not hold anymore. Since Eq. (52) is absent, there is still a residual particle-hole symmetry according to which

$$\delta_1 + \delta_2 = 0 \bmod(\pi).$$

If $\delta_1=-\delta_2$ then the two limiting cases, $\delta_1=\delta_2=0$ and $\delta_1=-\delta_2=\pi/2$, can be smoothly connected without requiring any critical point in between. This argument thus proves that an intermediate fixed point does not need to exist, yet it does not demonstrate its nonexistence. Indeed we know by bosonization and we now show by NRG that both Eqs. (53) and (54) do not wash out the UFP. In contrast a T^x term (54) does destabilize the fixed point, as shown later.

A direct way to prove that a particle-hole symmetry-breaking perturbation of the form (52) does not spoil the UFP is to analyze the low-energy spectrum. We show in Fig. 7 the analogy of Fig. 1 in the presence of a finite $\nu=0.05$, which breaks particle-hole symmetry. In spite of that, we still find evidences of an UFP separating the Kondo-screened from the unscreened regimes. Needless to say, this fixed point is identified by the same spectrum we find in the particle-hole symmetric case, as can be realized by comparing the intermediate crossover region in Fig. 7 with that in Fig. 1. Yet one might object that this is not a rigorous proof since numerically it is not possible to distinguish a true transition from a sharp crossover. Even though we did check that upon varying J we can approach as close as we want the UFP, eventually flowing in either of the two stable fixed points, we have found it more convenient to resort to an alternative proof that seems freer of numerical uncertainties.

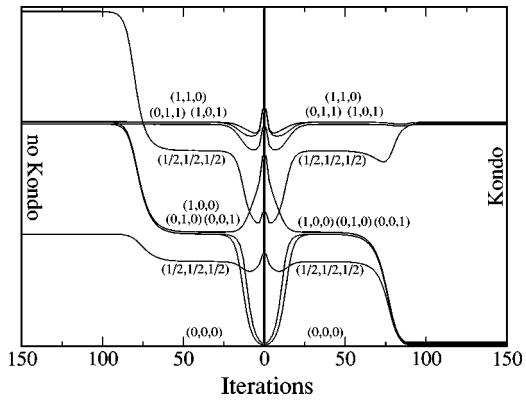

FIG. 7. Lowest-energy levels versus the chain size N in the presence of a finite $\nu=0.05$. The right/left panels correspond to a deviation $\delta J/J^*=\pm 3\times 10^{-5}$ from the fixed point value J^*. The levels are labeled by the quantum numbers (Q,T^z,S) as in Fig. 1. Notice that as a consequence of $\nu\neq 0$ some degeneracies found in the particle-hole symmetric case are lost.

Let us go back to Eq. (39) and try to guess how would it change in the presence of Eq. (52) and/or Eq. (53). We now introduce one S matrix for each channel, S_a with $a=1,2$, satisfying

$$\mathrm{Re}\, S_a(0) = \cos 2\delta_a(0) = 1 - 2\pi\Delta_0\rho_a(0). \tag{55}$$

Let us assume that, across the UFP, the zero-frequency phase shifts still jump by $\pi/2$. In other words, if we denote as

$$\delta_{-,a}(0) \equiv \delta_a \tag{56}$$

the phase shift in the unscreened phase, in the Kondo-screened phase the phase shift should be

$$\delta_{+,a}(0) = \delta_a + \frac{\pi}{2}.$$

Through Eq. (55) this would imply a jump of the DOS at the chemical potential given by

$$\rho_{+,a}(0) - \rho_{-,a}(0) = \frac{1}{\pi\Delta_0}\cos 2\delta_a = \rho_0 \cos 2\delta_a. \tag{57}$$

The above scenario predicts that although the pseudogap in the unscreened phase is partly filled away from particle-hole symmetry, the DOS has a finite jump across the UFP. This is indeed confirmed by NRG. In Fig. 8 we plot the DOS at fixed $\nu=0.05$, [see Eq. (52)], across the UFP, clearly showing the jump. We notice that if only Eq. (52) is present, then $\delta_1=\delta_2$ in Eq. (56). If Eq. (52) is absent but Eq. (53) is present, then $\delta_1=-\delta_2$, yet the behavior across the UFP is similar, which is the reason why we just show the results with finite ν. This behavior is also compatible with the NRG result that the charge and T^z Wilson ratios vanish around the UFP. Actually they all suggest that the model can absorb a chemical potential shift, equal or different in the two chan-

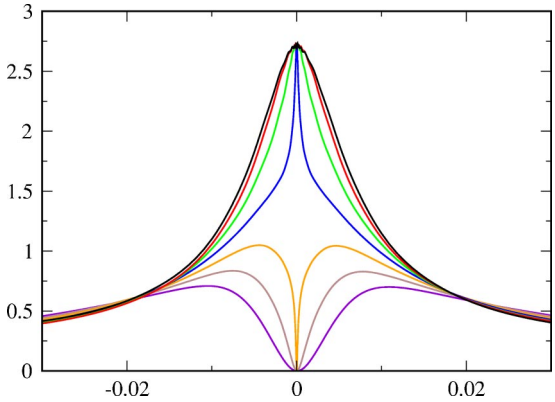

FIG. 8. (Color online) Impurity DOS across the UFP in the presence of a finite $\nu=0.05$, which breaks particle-hole symmetry. From top to bottom $J/J^*=0,0.28,0.57,0.86,1.14,1.43,1.71$. Notice that the DOS at the chemical potential is always finite, although very small and hence not visible in the figure. U and Δ_0 have the same values as in Fig. 5.

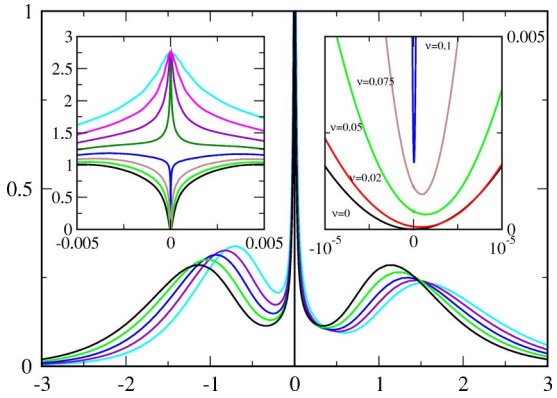

FIG. 9. (Color online) Impurity DOS upon increasing the strength of particle-hole symmetry breaking ν starting from the unscreened pseudogap phase ($\nu=0,0.05,0.1$) up to the Kondo-screened phase ($\nu=0.15,0.2$). In the left inset it is shown the low-energy part across the UFP (from top to bottom $\nu=0.2,0.175,0.15,0.125,0.1,0.075,0.05,0$); notice the analogy with the p-h symmetric case in Fig. 5. In the right inset we explicitly show the gradual filling of the pseudogap upon increasing ν. The values of U and Δ_0 are those of Fig. 5.

nels 1 and 2, on a high-energy scale, at least of order T_+, without having to modify what takes place at lower energies of order T_-: a kind of Anderson's compensation principle for our conserved quantities. Following these observations, we argue that the DOS for orbital $a=1,2$ in the presence of any of the two perturbations (52) and (53), assumed to be weak, can be modeled as

$$\rho_{\pm,a}(\epsilon)=\frac{\rho_a}{2}\left[\frac{T_+^2+\mu_{\pm,a}^2}{(\epsilon+\mu_{\pm,a})^2+T_+^2}\pm\cos 2\delta_a\frac{T_-^2}{\epsilon^2+T_-^2}\right], \quad (58)$$

where again the plus refers to the Kondo-screened phase and the minus to the unscreened phase, $\rho_a=\rho_{+,a}(0)$ is the value of the DOS at the chemical potential in the screened regime, while

$$\mu_{\pm,a}=\pm T_+\sin 2\delta_a.$$

According to the model DOS (58), the narrow peak and pseudogap remain pinned at the chemical potential, $\epsilon=0$, while only the broad resonance moves away from particle-hole symmetry.

Let us now study what happens if, starting from the particle-hole symmetric pseudogap phase, we move away by increasing ν, keeping all other Hamiltonian parameters fixed. As shown in Fig. 9, ν is able to drive the model across the UFP. This result could be foreseen. Indeed ν forces the impurity to accomodate $2-\nu$ electrons. If $\nu=1$, the impurity tends to be singly occupied. Therefore in the Kondo limit it behaves like a spin $S=1/2$ and pseudospin $T=1/2$ moment, which can be perfectly screened for the Kondo effect and is moreover stable with respect to little changes of ν with respect to $\nu=1$. Hence, if the model is at $\nu=0$ in the pseudogap phase, it has to cross a fixed point to reach the large-ν Kondo-screened regime. This behavior is quite interesting in connection with DMFT lattice calculations, since it implies that the lattice-model local critical regime, which reflects the single-impurity UFP, may also be attained by doping, as recently confirmed.[9]

In conclusion we find that the UFP extends away from the particle-hole symmetric point, $\nu=0$, giving rise to a whole critical line, $J_*(\nu,\Delta_0,U)<0$ such that for $J>J_*(\nu,\Delta_0,U)$ complete Kondo screening takes place while for $J<J_*(\nu,\Delta_0,U)$ the impurity is in the unscreened pseudogap regime. Let us briefly discuss the fate of this critical line as particle-hole asymmetry becomes very large. We find that $J_*(\nu,\Delta_0,U)$ decreases by increasing ν, being of order $-T_K$ for $\mu\simeq 0$ and becoming of order $-U$ for large $|\nu|$, thus eventually going outside the region $U\gg|J|,\Delta_0$ we are interested in. This result can also be physically understood. Let us suppose for instance that the average impurity occupancy is fixed as one. Still we keep assuming $U\gg\Delta_0$, thus preventing the occupancy from freely fluctuating around its mean value. We notice that the effective Hubbard repulsion, U_{eff}, acting on the impurity is by definition $U_{eff}\equiv E_0(0)+E_0(2)-2E_0(1)$, where $E_0(n)$ is the ground-state energy for n-electron configurations. If $J<0$, the $n=2$ ground state has $S=0$, $T=1$, and $T_z=0$ [see Eq. (5)], and we find $U_{eff}=U-2|J|$. Therefore, if $U\gg|J|$, the impurity effectively behaves like a spin $S=1/2$ and pseudospin $T=1/2$ moment, which, as we said, is Kondo screened. In contrast, if $J\ll -U$, $U_{eff}\ll 0$ and hence the impurity prefers to oscillate bewteen zero and double occupancy to take full advantage of the inverted Hund's rules. In this unconventional mixed-valence regime induced by J, the DOS actually develops a pseudogap at the chemical potential. Therefore the critical line transforms for large particle-hole asymmetry into the critical point, which separates the local moment from the J-induced mixed valence regime.

A completely different behavior occurs if we introduce instead a T^x perturbation of the form (54). Here, as expected, we do not find any jump of the DOS, as clear in Fig. 10 where we compare the DOS at the chemical potential in the presence either of Eq. (52), $h_{p\text{-}h}\neq 0$, or Eq. (54), $h_x\neq 0$. This demonstrates that a perturbation in the particle-hole channel that breaks the orbital U(1) symmetry is relevant at the UFP,

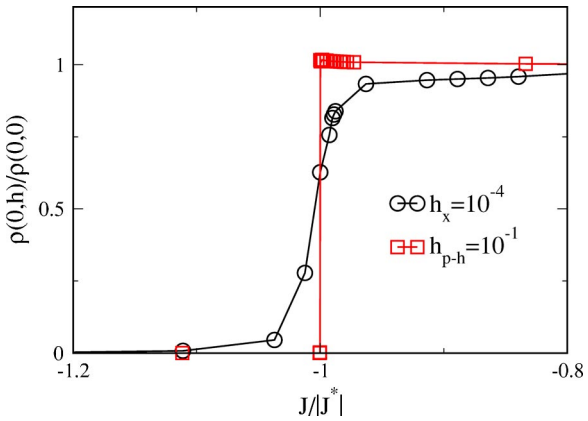

FIG. 10. (Color online) Comparison of the DOS values at the chemical potential as function of J either in the presence of a finite particle-hole symmetry breaking h_{p-h}, $\rho(0,h_{p-h})$, or of a T^x symmetry breaking h_x, $\rho(0,h_x)$, normalized to their values at $J=0$. Notice that h_x, although three orders of magnitude smaller than h_{p-h}, washes out the DOS jump, contrary to h_{p-h}.

unlike Eq. (52) and (53), which instead do not break the $U(1)_{orbit}$ symmetry.

Finally let us discuss what happens in the AIM, which corresponds within DMFT to two Hubbard planes coupled by a transverse hopping, Eq. (18), with $J=V=0$ plus the term (19). We already noticed that $t_\perp$ plays an ambiguous role. It generates an antiferromagnetic exchange, $J=4t_\perp^2/U$, which may stabilize an UFP, but it also induces a relevant T^x perturbation [see Eq. (20)]. Since the UFP is never reachable, the model always flows to a Fermi-liquid fixed point. In the presence of $t_\perp$ it is more appropriate to introduce the even and odd combinations of the orbitals 1 and 2:

$$d_{e\sigma} = \frac{1}{\sqrt{2}}(d_{1\sigma} + d_{2\sigma}),$$

$$d_{o\sigma} = \frac{1}{\sqrt{2}}(d_{1\sigma} - d_{2\sigma}),$$

and correspondingly the even and odd conduction-electron scattering channels. According to what we said at the beginning of this section, we expect the phase shifts $\delta_e = -\delta_o$ to be smooth functions of J. If there were no remnant of the UFP, the DOS's should simply show a resonance, the even channel above the chemical potential and the odd channel below it. In reality the behavior of the DOS remains strongly influenced by the UFP, even though never reachable. This is evident in Fig. 11, where we draw the DOS of $d_{e\sigma}$, $\rho_e(\epsilon)$ (the odd one is simply obtained by reflection around zero energy), at fixed $t_\perp$ upon varying the hybridization width Δ_0. There is no point at which the DOS jumps at the chemical potential, yet a partly filled asymmetric pseudogap remains. In Fig. 12 we draw the low-energy difference between the even and odd DOS's, which is also the off-diagonal spectral function $A_{12}(\epsilon)$. $A_{12}(\epsilon)$ shows a low-energy feature that has a nonmonotonic behavior in Δ_0 and almost develops into a singularity around $\Delta_0 = 0.47$. We think that these results bring to the fore that $t_\perp$

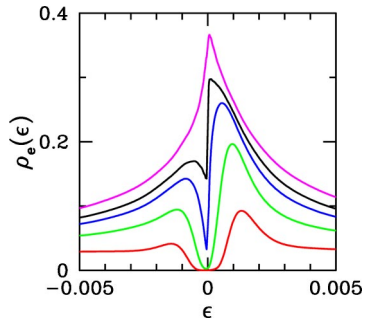

FIG. 11. (Color online) Impurity DOS of $d_{e\sigma}$, $\rho_e(\epsilon)$, for the AIM Eq. (20). The different curves correspond from the top to the bottom to values of $\Delta_0 = 0.5, 0.47, 0.45, 0.4, 0.3$ with $t_\perp = 0.05$ and $U=8$. These values correspond to $J_K = 0.08, 0.075, 0.072, 0.064, 0.049$ and $J = 4t_\perp^2/U = 0.00125$. We notice the remnant of an asymmetric pseudogap of order J.

alone is able to drive the model very close to the UFP. In other words, the width of the critical region is larger than the energy scale that cuts off the fixed-point singularities, although both are generated by the same $t_\perp$.

VIII. CONCLUSIONS

In this work we have analyzed the spectral properties of the two-orbital Anderson impurity model, Eq. (1), which includes an exchange splitting J, which favors, if negative, a nondegenerate impurity configuration. This model was already shown in Ref. 8 to possess a non-Fermi-liquid fixed point that separates a phase where conventional Kondo screening takes place from an unscreened phase in which J takes care of quenching the impurity degrees of freedom.

The impurity density of states has the following behavior across the fixed point in the presence of particle-hole symmetry. In the Kondo-screened phase it displays a conventional very narrow Kondo resonance on top of a broader resonance. In contrast, in the unscreened phase a narrow pseudogap appears within the broad resonance. At the fixed point only the latter survives. Away from half-filling, the

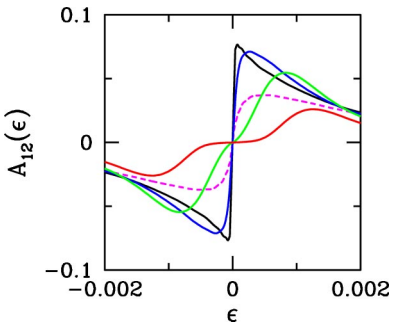

FIG. 12. (Color online) Off-diagonal spectral function, $A_{12}(\epsilon)$, with $t_\perp = 0.05$. The different solid curves correspond from the top to the bottom for $\epsilon > 0$ to values of $\Delta_0 = 0.47, 0.45, 0.4, 0.3$, while the dashed curve corresponds to $\Delta_0 = 0.5$. We notice that the low-energy feature first moves towards zero energy when Δ_0 increases from 0.3 to 0.47, but from 0.47 to 0.5 it goes back again. Moreover, around $\Delta_0 = 0.47$, $A_{12}(\epsilon)$ is almost singular.

pseudogap remains pinned at the chemical potential, although it gets partly filled. Yet there is still a fixed point across which the density of states at the chemical potential jumps. Finally we have explicitly shown that the intermediate fixed point is unstable towards physical symmetry breaking fields, which include both particle-hole and particle-particle channels. The relevance of this impurity model for dynamical mean field theory calculations has been already emphasized in Ref. 8 and confirmed by Refs. 9 and 11. Here we would like to clarify some aspects in view of the newly discovered spectral properties.

As discussed in Ref. 8, any lattice model that maps by DMFT onto the impurity model (1) plus (13) should encounter the unstable fixed point before the Mott transition, namely, when the effective quasiparticle bandwidth becomes of the order of $|J|$. However the instability of the single-impurity fixed point should likely transform into a bulk instability through the DMFT self-consistency conditions. As we showed there are several competing physical instabilities around the fixed point, in the particle-hole and particle-particle channels. In the absence of nesting or van Hove singularities, we argued in Ref. 8 that the particle-particle channel dominates, leading to a superconducting pocket just before the Mott transition, which has been indeed observed by DMFT.[9] However, there might be physically relevant cases where those band-structure singularities occur, which would favor a uniform or modulated order parameter in one of the particle-hole unstable channels. What should we expect upon moving away from these peculiar cases, for instance by doping? Clearly the band-structure singularities weakens upon doping. Yet the fixed point is not washed out away from particle-hole symmetry. We showed in fact that the pseudogap remains pinned at the chemical potential. We believe that this would result in competition between particle-hole and particle-particle channels that gradually turns in favor of the latter, thus predicting a particle-hole order parameter that dies out upon doping in favor of a superconducting one.

Equally interesting is what we find for the Anderson impurity model, which corresponds within DMFT to two Hubbard planes, with large in-plane coordination, coupled by a hopping term $t_\perp$, Eq. (18), with $J=V=0$ plus the term (19). Here the physics is not as transparent as in the model (1), essentially because $t_\perp$ provides at the same time a mechanism for the existence of a fixed point as well as for its instability. However, the numerical renormalization group results for the single-impurity show evidence that an almost critical region does exist, in spite of the fact that the nontrivial fixed point can never be attained. This suggests that the physics of the two coupled Hubbard planes close to the Mott transition may still be influenced by the single-impurity fixed point.

Finally, we briefly comment what our results would imply for the model with conventional Hund's rules [see Eq. (16)]. This case in the absence of single-ion anisotropy corresponds to a Kondo-screened regime where, as we showed in Fig. 4, the spin-triplet Cooper channel is attractive. By increasing the Hubbard U in the lattice model, the Kondo temperature of the effective AIM decreases, which implies that the spin-triplet dimensionless scattering amplitude gradually also decreases, (see Fig. 4) for increasing $J>0$. This suggests that the instability towards spin-triplet superconductivity may actually be enhanced by strong correlations, compatible with recent DMFT calculations.[11] In addition, we would expect that, in the presence of a single-ion anisotropy, $D>0$ in Eq. (16), the enhancement of spin-triplet superconductivity might be even more dramatic.

ACKNOWLEDGMENTS

We are very grateful to G. Zaránd, M. Sindel, and C. Castellani for their useful advice. We thank M. Capone, P. Nozières, G.E. Santoro, and E. Tosatti for helpful discussions. This work has been partly supported by MIUR COFIN and FIRB RBAU017S8R004.

APPENDIX. FERMI-LIQUID THEORY OF THE ANDERSON IMPURITY MODEL

In this appendix we build up a Fermi-liquid theory of our AIM closely following the conventional approach (see for instance Ref. 21). Our purpose is twofold. First the Fermi-liquid theory provides a framework to analyze the NRG data. Moreover, it allows us to introduce within DMFT the concept of a local Fermi-liquid description in addition to the conventional one, which refers instead to low-frequency and momentum scattering amplitudes.

Let us consider more generally a multiorbital Anderson impurity model. As in our case, we assume that besides spin rotational symmetry also orbital degeneracy is preserved, so that the fully interacting impurity Green's functions are diagonal and independent of both spin and orbital indices.

The variation of the electron number with orbital symmetry a and spin α associated with the presence of the impurity is given by[21]

$$\Delta n_{a\alpha} = \oint \frac{dz}{2\pi i} f(z) \frac{\partial}{\partial z} \ln G_{a\alpha}(z),$$

where the integration contour encloses the real axis clockwise, $f(z)$ is the Fermi distribution function in the complex plane, and $G_{a\alpha}$ the impurity single-particle Green's function. Since the Green's function has a branch cut on the real axis, the above expression is also equal to

$$\Delta n_{a\alpha} = -\frac{1}{\pi} \int_{-\infty}^{\infty} d\epsilon \frac{\partial f(\epsilon)}{\partial \epsilon} \mathrm{Im} \ln G_{a\alpha}(\epsilon + i\delta), \qquad \text{(A1)}$$

with δ an infinitesimal positive number. The impurity density of states is further determined through

$$\rho_{a\alpha}(\epsilon) = -\frac{1}{\pi} \mathrm{Im}\, G_{a\alpha}(i\omega_n \to \epsilon + i\delta). \qquad \text{(A2)}$$

If we introduce a source field in the Hamiltonian by

$$\delta\hat{H} = -\sum_{a\alpha} h_{a\alpha}\, n_{a\alpha},$$

where

$$n_{a\alpha} = \sum_{\mathbf{k}} c^{\dagger}_{\mathbf{k}\ a\alpha} c_{\mathbf{k}\ a\alpha} + d^{\dagger}_{a\alpha} d_{a\alpha},$$

then

$$G_{a\alpha}(i\omega_n)^{-1} \rightarrow i\omega_n + h_{a\alpha} - \Delta_{a\alpha}(i\omega_n, h_{a\alpha}) - \Sigma_{a\alpha}(i\omega_n, \{h_{b\beta}\}),$$

where

$$\Delta_{a\alpha}(i\omega_n, h_{a\alpha}) = \sum_{\mathbf{k}} |V_{\mathbf{k}}|^2 \frac{1}{i\omega_n - \epsilon_{\mathbf{k}} + h_{a\alpha}},$$

is the hybridization function in the presence of the source. Therefore the derivative with respect to the external field of the variation of the electron number associated with the impurity is given by

$$\left(\frac{\partial \Delta n_{a\alpha}}{\partial h_{b\beta}}\right)_{h=0} = \int_{-\infty}^{\infty} \frac{d\epsilon}{\pi} \frac{\partial f(\epsilon)}{\partial \epsilon} \mathrm{Im}\Bigg(G(\epsilon + i\delta) \times \Bigg\{ \delta_{ab}\delta_{\alpha\beta}\left[1 - \left(\frac{\partial \Delta(z)}{\partial z}\right)_{z=\epsilon+i\delta}\right] - \left(\frac{\partial \Sigma_{a\alpha}(\epsilon + i\delta)}{\partial h_{b\beta}}\right)_{h=0} \Bigg\} \Bigg), \tag{A3}$$

where $\Sigma_{a\alpha}(i\omega_n)$ is the impurity self-energy and we made use of

$$\left(\frac{\partial \Delta_{a\alpha}(z, h_{a\alpha})}{\partial h_{b\beta}}\right)_{h=0} = \delta_{ab}\delta_{\alpha\beta} \frac{\partial \Delta(z)}{\partial z},$$

$\Delta(z)$ being the hybridization function in the absence of h. On the other hand,

$$\left(\frac{\partial \Sigma_{a\alpha}(i\omega_n)}{\partial h_{b\beta}}\right)_{h=0} = -\frac{1}{\beta} \sum_m \sum_{b\beta} \Gamma_{a\alpha,b\beta;b\beta,a\alpha}(i\omega_n, i\epsilon_m; i\epsilon_m, i\omega_n) \times G(i\epsilon_m)^2 \left(1 - \frac{\partial \Delta(i\epsilon_m)}{\partial i\epsilon_m}\right), \tag{A4}$$

where we used the property that, at $h=0$, the Green's function does not depend on a and α. The interaction vertex is the reducible one.

Let us assume that there exists a set of conserved operators

$$\mathcal{M}^{(i)} = \sum_{\mathbf{k}} \sum_{ab\alpha\beta} c^{\dagger}_{\mathbf{k}a\alpha} (\hat{M}^{(i)})^{\alpha\beta}_{ab} c_{\mathbf{k}\ b\beta} + \sum_{ab\alpha\beta} d^{\dagger}_{a\alpha} (\hat{M}^{(i)})^{\alpha\beta}_{ab} d_{b\beta},$$

where $\hat{M}^{(i)}$ are Hermitean matrices and the suffix i identifies the particular conserved operator. For convenience we adopt the normalization $\mathrm{Tr}(\hat{M}^{(i)} \cdot \hat{M}^{(i)}) = 1$. Then, if we add a source field

$$\delta\hat{H} = -h^{(i)} \mathcal{M}^{(i)},$$

we can use the basis that diagonalizes $\hat{M}^{(i)}$ and apply the above results to find the variation of $\langle \mathcal{M}^{(i)} \rangle$ associated with the presence of the impurity at first order in the applied field. Going back to the original basis, we would find the following expression of the difference $\delta\chi^{(i)}$ between the susceptibilities in the presence and absence of the impurity:

$$\delta\chi^{(i)} = \delta\left(\frac{\partial \langle \mathcal{M}^{(i)} \rangle}{\partial h^{(i)}}\right)_{h=0} = \int_{-\infty}^{\infty} \frac{d\epsilon}{\pi} \frac{\partial f(\epsilon)}{\partial \epsilon} \mathrm{Im} \Bigg\{ G(\epsilon + i\delta) \times \Bigg[1 - \left(\frac{\partial \Delta(i\epsilon)}{\partial i\epsilon}\right)_{i\epsilon=\epsilon+i\delta} + \frac{1}{\beta} \sum_n \sum_{abcd} \sum_{\alpha\beta\gamma\delta} \Gamma_{b\beta,d\delta;c\gamma,a\alpha}(\epsilon + i\delta, i\epsilon_n; i\epsilon_n, \epsilon + i\delta) \times (\hat{M}^{(i)})^{\alpha\beta}_{ab} (\hat{M}^{(i)})^{\gamma\delta}_{cd} G(i\epsilon_n)^2 \left(1 - \frac{\partial \Delta(i\epsilon_m)}{\partial i\epsilon_m}\right) \Bigg] \Bigg\}. \tag{A5}$$

Hereafter we drop the subscript i. One can demonstrate that the following Ward identities hold for the impurity:

$$[\Sigma(i\epsilon + i\omega) - \Sigma(i\epsilon)]\, M^{\alpha\beta}_{ab} = -\frac{1}{\beta} \sum_n \sum_{cd;\gamma\delta} \Gamma_{a\alpha,d\delta;c\gamma,b\beta}(i\epsilon + i\omega, i\epsilon_n; i\epsilon_n + i\omega, i\epsilon) \times M^{\gamma\delta}_{cd}\, G(i\epsilon_n + i\omega) G(i\epsilon_n) [i\omega - \Delta(i\epsilon_n + i\omega) + \Delta(i\epsilon_n)]. \tag{A6}$$

It then follows that

$$\frac{\partial \Sigma(i\epsilon)}{\partial i\epsilon} M^{\alpha\beta}_{ab} = -\frac{1}{\beta} \sum_n \sum_{cd} \sum_{\gamma\delta} \Gamma_{a\alpha,d\delta;c\gamma,b\beta}(i\epsilon, i\epsilon_n; i\epsilon_n, i\epsilon) M^{\gamma\delta}_{cd}\, G(i\epsilon_n)^2 - \lim_{i\omega\rightarrow 0} \frac{1}{\beta} \sum_n \sum_{cd;\gamma\delta} \Gamma_{a\alpha,d\delta;c\gamma,b\beta}(i\epsilon + i\omega, i\epsilon_n; i\epsilon_n + i\omega, i\epsilon) \times M^{\gamma\delta}_{cd}\, G(i\epsilon_n + i\omega) G(i\epsilon_n) \frac{[-\Delta(i\epsilon_n + i\omega) + \Delta(i\epsilon_n)]}{i\omega}$$

$$= -\frac{1}{\beta} \sum_n \sum_{cd} \sum_{\gamma\delta} \Gamma_{a\alpha,d\delta;c\gamma,b\beta}(i\epsilon, i\epsilon_n; i\epsilon_n, i\epsilon) M^{\gamma\delta}_{cd}\, G(i\epsilon_n)^2 \left(1 - \frac{\partial \Delta(i\epsilon_n)}{\partial i\epsilon_n}\right) + \int_{-\infty}^{\infty} \frac{d\epsilon'}{2\pi} \frac{\partial f(\epsilon')}{\partial \epsilon'} \sum_{cd;\gamma\delta} \Gamma_{a\alpha,d\delta;c\gamma,b\beta}(i\epsilon, \epsilon' - i\delta'; \epsilon' + i\delta', i\epsilon) \times (M^{(i)})^{cd}_{\gamma\delta} (M^{(i)})^{\beta\alpha}_{ba} G(\epsilon' + i\delta') G(\epsilon' - i\delta') \mathrm{Im}[\Delta(\epsilon' - i\delta') - \Delta(\epsilon' + i\delta')]. \tag{A7}$$

Let us define the quantity

$$\overline{\rho_*} = \int_{-\infty}^{\infty} \frac{d\epsilon}{\pi} \frac{\partial f(\epsilon)}{\partial \epsilon} \mathrm{Im}\left\{ G(\epsilon + i\delta)\left[1 - \left(\frac{\partial \Delta(i\epsilon)}{\partial i\epsilon} \right)_{i\epsilon \to \epsilon + i\delta} - \left(\frac{\partial \Sigma(i\epsilon)}{\partial i\epsilon} \right)_{i\epsilon \to \epsilon + i\delta} \right] \right\}, \tag{A8}$$

which plays the role of the quasiparticle DOS at the chemical potential. Then, through Eqs. (A5), (A7), and (A8), the following equation is readily found:

$$\begin{aligned}
\overline{\rho_*} &= \sum_{ab} \sum_{\alpha\beta} \overline{\rho_*} (\hat{M}^{(i)})^{\beta\alpha}_{ba} (\hat{M}^{(i)})^{\alpha\beta}_{ab} \\
&= \delta\chi^{(i)} - \frac{1}{2\pi^2} \int_{-\infty}^{\infty} d\epsilon d\epsilon' \frac{\partial f(\epsilon)}{\partial \epsilon} \frac{\partial f(\epsilon')}{\partial \epsilon'} \mathrm{Im}\left\{ G(\epsilon + i\delta) \left[\sum_{cd;\gamma\delta} \Gamma_{a\alpha,d\delta;c\gamma,b\beta}(\epsilon + i\delta, \epsilon' - i\delta'; \epsilon' + i\delta', \epsilon + i\delta) \right.\right. \\
&\quad \left.\left. \times (M^{(i)})^{\gamma\delta}_{cd} (M^{(i)})^{\beta\alpha}_{ba} G(\epsilon' + i\delta') G(\epsilon' - i\delta') \mathrm{Im}[\Delta(\epsilon' - i\delta') - \Delta(\epsilon' + i\delta')] \right] \right\} \\
&= \delta\chi^{(i)} + \frac{1}{2\pi} \int_{-\infty}^{\infty} d\epsilon d\epsilon' \frac{\partial f(\epsilon)}{\partial \epsilon} \frac{\partial f(\epsilon')}{\partial \epsilon'} \rho(\epsilon) \sum_{cd;\gamma\delta} \Gamma_{a\alpha,d\delta;c\gamma,b\beta}(\epsilon + i\delta, \epsilon' - i\delta'; \epsilon' + i\delta', \epsilon + i\delta) \\
&\quad \times (M^{(i)})^{\gamma\delta}_{cd} (M^{(i)})^{\beta\alpha}_{ba} G(\epsilon' + i\delta') G(\epsilon' - i\delta') \mathrm{Im}[\Delta(\epsilon' - i\delta') - \Delta(\epsilon' + i\delta')].
\end{aligned} \tag{A9}$$

The last expression is obtained by noticing that only the imaginary part of $G(\epsilon + i\delta)$ contributes, where $\mathrm{Im}\, G(\epsilon + i\delta) = -\pi\rho(\epsilon)$. Equation (A9) allows us to express any susceptibility to fields coupled to conserved quantities. If the hybridization function is smooth at low energies, then

$$\Delta(\epsilon' - i\delta') - \Delta(\epsilon' + i\delta') \simeq 2i\Delta_0,$$

and hence we can rewrite (A9) as follows:

$$\begin{aligned}
\delta\chi^{(i)} &= \overline{\rho_*} \left[1 - \frac{\Delta_0}{\overline{\rho_*}\pi} \int_{-\infty}^{\infty} d\epsilon d\epsilon' \frac{\partial f(\epsilon)}{\partial \epsilon} \rho(\epsilon) \frac{\partial f(\epsilon')}{\partial \epsilon'} \right. \\
&\quad \times \sum_{cd;\gamma\delta} \Gamma_{a\alpha,d\delta;c\gamma,b\beta}(\epsilon + i\delta, \epsilon' - i\delta'; \epsilon' + i\delta', \epsilon + i\delta) \\
&\quad \left. \times (M^{(i)})^{\gamma\delta}_{cd} (M^{(i)})^{\beta\alpha}_{ba} G(\epsilon' + i\delta') G(\epsilon' - i\delta') \right], \\
&\equiv \overline{\rho_*}[1 - A_i],
\end{aligned} \tag{A10}$$

which allows us to identify local Landau A parameters through

$$\begin{aligned}
A_i &= \frac{\Delta_0}{\overline{\rho_*}\pi} \int_{-\infty}^{\infty} d\epsilon d\epsilon' \frac{\partial f(\epsilon)}{\partial \epsilon} \rho(\epsilon) \frac{\partial f(\epsilon')}{\partial \epsilon'} \\
&\quad \times \sum_{cd;\gamma\delta} \Gamma_{a\alpha,d\delta;c\gamma,b\beta} \\
&\quad \times (\epsilon + i\delta, \epsilon' - i\delta'; \epsilon' + i\delta', \epsilon + i\delta) (M^{(i)})^{\gamma\delta}_{cd} (M^{(i)})^{\beta\alpha}_{ba} \\
&\quad \times G(\epsilon' + i\delta') G(\epsilon' - i\delta').
\end{aligned} \tag{A11}$$

The above expression is quite general but simplifies substantially when the imaginary part of the impurity self-energy vanishes at low real frequency. In this case

$$G(i\epsilon_n \to \pm i0^+) = \frac{1}{-\epsilon_d \pm i\Delta_0},$$

where $\epsilon_d = \epsilon_d^{(0)} + \mathrm{Re}\,\Sigma(0)$ is the actual position of the d resonance. Then, through Eq. (A2),

$$\rho(0) = \frac{1}{\pi} \frac{\Delta_0}{\epsilon_d^2 + \Delta_0^2} = \frac{\Delta_0}{\pi} G(i0^+) G(i0^-). \tag{A12}$$

Analogously

$$\overline{\rho_*} = \frac{\rho(0)}{Z}, \quad \frac{1}{Z} = 1 - \left(\frac{\partial \Sigma(i\epsilon)}{\partial i\epsilon} \right)_{i\epsilon \to i0^+}$$

and hence

$$A_i = \sum_{abcd} \sum_{\alpha\beta\gamma\delta} [Z^2 \overline{\rho_*} \Gamma_{a\alpha,d\delta;c\gamma,b\beta}(0,0;0,0)] (\hat{M}^{(i)})^{\beta\alpha}_{ba} (\hat{M}^{(i)})^{\gamma\delta}_{cd}, \tag{A13}$$

which is the more conventional expression of the Landau parameters.[21] Although the above equation is a particular case of the general one (A11), to simplify the notations in what follows we will use Eq. (A13) as a shorthand expression of Eq. (A11).

IX. Application to the twofold orbitally degenerate AIM

Let us now apply the above results to our model. An incoming pair can be a spin triplet, orbital singlet, with a scattering vertex at zero incoming and outgoing frequencies given by

$$\Gamma^1 \to \Gamma_{1\sigma,2\sigma;2\sigma,1\sigma}, \quad \frac{1}{2}\Gamma_{1\sigma,2-\sigma;2-\sigma,1\sigma} - \frac{1}{2}\Gamma_{1\sigma,2-\sigma;1-\sigma,2\sigma}.$$

Here 1 and 2 label the two orbitals with $T^z = +1/2$ and $T^z = -1/2$, respectively. Alternatively it can be a spin singlet, orbital triplet with $T^z = 0$, with scattering vertex

$$\Gamma_0^0 \to \frac{1}{2}\Gamma_{1\sigma,2-\sigma;2-\sigma,1\sigma} + \frac{1}{2}\Gamma_{1\sigma,2-\sigma;1-\sigma,2\sigma},$$

or with $T^z = \pm 1$, in which case

$$\Gamma_\pm^0 \to \Gamma_{1\sigma,1-\sigma;1-\sigma,1\sigma},\ \Gamma_{2\sigma,2-\sigma;2-\sigma,2\sigma}.$$

In reality it is more convenient to introduce the dimensionless scattering vertices:

$$\mathcal{A}^1 = Z^2\overline{\rho_*}\Gamma_1 = Z\rho(0)\Gamma^1,$$

$$\mathcal{A}_0^0 = Z^2\overline{\rho_*}\Gamma_0^0 = Z\rho(0)\Gamma_0^0,$$

$$\mathcal{A}_\pm^0 = Z^2\overline{\rho_*}\Gamma_\pm^0 = Z\rho(0)\Gamma_\pm^0. \tag{A14}$$

As we previously showed, only the susceptibilities of conserved quantities can be expressed in terms of the Landau parameters (A13), which are simply connected with the scattering vertices at zero frequency. Yet we can still define Landau parameters for nonconserved quantities, which, although they do not serve to calculate susceptibilities, may provide a qualitative estimate of their magnitude. Therefore we are going to introduce the Landau parameters for the charge, A_C, spin A_S, the z component of the pseudospin $\vec{T}$, $A_T^{\|}$, all being related to conserved quantities, but also for the x and y components of $\vec{T}$, $A_T^{\perp}$, as well as for the spin-orbital components, $A_{ST}^{\|}$ and $A_{ST}^{\perp}$. In terms of the dimensionless amplitudes (A14) they can be shown, after some lengthy algebra, to have the following expressions:

$$A_C = \frac{1}{4}(6\mathcal{A}^1 + 2\mathcal{A}_0^0 + 4\mathcal{A}_\pm^0), \tag{A15}$$

$$A_S = \frac{1}{4}(2\mathcal{A}^1 - 2\mathcal{A}_0^0 - 4\mathcal{A}_\pm^0), \tag{A16}$$

$$A_T^{\|} = \frac{1}{4}(-6\mathcal{A}^1 - 2\mathcal{A}_0^0 + 4\mathcal{A}_\pm^0), \tag{A17}$$

$$A_T^{\perp} = \frac{1}{4}(-6\mathcal{A}^1 + 2\mathcal{A}_0^0), \tag{A18}$$

$$A_{ST}^{\|} = \frac{1}{4}(-2\mathcal{A}^1 + 2\mathcal{A}_0^0 - 4\mathcal{A}_\pm^0), \tag{A19}$$

$$A_{ST}^{\perp} = \frac{1}{4}(-2\mathcal{A}^1 - 2\mathcal{A}_0^0). \tag{A20}$$

Let us consider several possible cases.

(1) If $J=0$, SU(4) symmetry holds. Then $\mathcal{A}^1 = \mathcal{A}_0^0 = \mathcal{A}_\pm^0 = A$, leading to

$$A_C = 3A,$$

$$A_S = A_T^{\|} = A_T^{\perp} = A_{ST}^{\|} = A_{ST}^{\perp} = -A.$$

In the *s-d* limit, when the AIM maps onto a SU(4) Kondo model, the charge compressibility in negligible, leading to $3A=1$. The Wilson ratios for the conserved quantities are defined trough

$$R_i = \frac{\delta\chi^{(i)}}{\chi_0}\frac{C_V}{\delta C_V} = 1 - A_i,$$

where $\delta\chi^{(i)}$ has been defined in (A5), $\chi_0 = \rho_c$ and C_V are, respectively, the conduction-electron susceptibility and specific heat in the absence of the impurity, and

$$\delta C_V = \frac{\overline{\rho_*}}{\rho_c} C_V,$$

is the variation of the specific heat due to the impurity. Hence all Wilson ratios have a universal value,

$$R_S = R_T = R_{ST} = 1 - A = 4/3, \tag{A21}$$

in agreement with conformal field theory.

(2) If $J \gg T_K > 0$ the impurity gets frozen in the Kondo limit into a spin $S=1$. Then both $A_C=1$ and $A_T^{\|}=1$, which implies

$$\mathcal{A}_\pm^0 = 1,$$

$$\mathcal{A}_0^0 = -3\mathcal{A}^1.$$

However one expects that, the spin triplet being an orbital singlet, the SU(2) orbital symmetry gets restored at the fixed point, much in the same way as spin anisotropy is irrelevant at the Kondo fixed point. This further implies that

$$\mathcal{A}_0^0 = -3\mathcal{A}^1 = 1,$$

namely, $A_S = -5/3$, with a Wilson ratio $R_S = 8/3$, in agreement with known results.

(3) Let us now suppose we are close to the UFP within the Kondo-screened regime. As usual the charge degrees of freedom are suppressed already below U, so that we can still assume $A_C=1$. Moreover, we expect that the spin and the orbital degrees of freedom related to T^z get quenched below T_+, while the remaining ones only below $T_- \ll T_+$. Therefore at very low temperatures $T < T_-$, we can safely assume that

$$T_-\delta\chi_S \sim T_-\delta\chi_T^{\|} \sim \frac{T_-}{T_+} \sim 0,$$

namely $A_S = A_T^{\|} = 1$. As a result we find that

$$\mathcal{A}_\pm^0 = \mathcal{A}^1 = 1, \tag{A22}$$

$$\mathcal{A}_0^0 = -3. \tag{A23}$$

Equation (A23) implies a strongly attractive *s*-wave singlet channel. The other Landau parameters are thus given by

$$A_T^{\perp} = A_{ST}^{\|} = -3, \tag{A24}$$

$$A_{ST}^{\perp} = 1. \tag{A25}$$

This further proves that the fixed point is equally unstable in the *s*-wave Cooper channel Γ_0^0, as well as in the T^x, T^y, and $\vec{S}T^z$ particle-hole channels. We finally notice that, although the Landau A parameters would suggest that the susceptibili-

ties in the unstable channels, all of which correspond to non-conserved quantities, diverge as $1/T_-$, in reality they only diverge logarithmically.[4,14,15] This is not incompatible with Fermi-liquid theory, which allows us to express in terms of the A parameters only those response functions related to conserved quantities.

Let us now use our model self-energy to extract some additional information. Through Eq. (45), we find that in the Kondo screened regime the expression (A13) holds with a quasiparticle residue

$$\frac{1}{Z}=\frac{\Delta_0}{2}\left(\frac{1}{T_+}+\frac{1}{T_-}\right). \tag{A26}$$

Indeed $Z\sim 2T_-/\Delta_0\to 0$ upon approaching the unstable fixed point.

On the contrary, the general expression (A11) has to be used inside the non-Kondo screened pseudo-gap phase. Through Eq. (44) for $G_-(i\epsilon_n)$ we find that at low frequency

$$G_-(\epsilon+i\delta)G_-(\epsilon-i\delta)\simeq\frac{1}{4\Delta_0^2}\frac{\epsilon^2(T_+-T_-)^2}{T_+^2T_-^2}$$
$$\simeq\frac{\pi}{2\Delta_0}\rho_-(\epsilon)\frac{T_+-T_-}{T_++T_-}.$$

By Eq. (46) the quasiparticle DOS at the chemical potential turns out to be finite,

$$\overline{\rho}_*=\frac{1}{\pi}\frac{T_++T_-}{T_+T_-}, \tag{A27}$$

even though the impurity DOS vanishes. In conclusion, within the pseudogap phase the Landau parameters have the following expression

$$A_i=\frac{\pi}{2}\frac{T_+T_-(T_+-T_-)}{(T_++T_-)^2}\int_{-\infty}^{\infty}d\epsilon d\epsilon'\frac{\partial f(\epsilon)}{\partial\epsilon}\rho(\epsilon)\frac{\partial f(\epsilon')}{\partial\epsilon'}\rho(\epsilon')$$
$$\times\sum_{cd;\gamma\delta}\Gamma_{a\alpha,d\delta;c\gamma,b\beta}(\epsilon+i\delta,\epsilon'-i\delta';\epsilon'+i\delta',\epsilon+i\delta)$$
$$\times(M^{(i)})^{\gamma\delta}_{cd}(M^{(i)})^{\beta\alpha}_{ba}. \tag{A28}$$

In spite of the anomalous impurity Green's function, the low-energy behavior should still be described within a local Fermi-liquid scenario by finite Landau parameters A_i's. Therefore, since the impurity DOS vanishes quadratically in the pseudogap phase, then the scattering vertices must display a singular behavior

$$\Gamma(\epsilon,\epsilon';\epsilon',\epsilon)\sim\frac{1}{(\epsilon+\epsilon')^4},$$

to compensate for the vanishing DOS's and provide finite A's.

[1] P. Nozières and A. Blandin, J. Phys. (Paris) **41**, 193 (1980).
[2] B. A. Jones and C. M. Varma, Phys. Rev. Lett. **58**, 843 (1987); B. A. Jones, C. M. Varma, and J. W. Wilkins, *ibid.* **61**, 125 (1988); B. A. Jones and C. M. Varma, Phys. Rev. B **40**, 324 (1989).
[3] I. Affleck and A. W. W. Ludwig, Phys. Rev. Lett. **68**, 1046 (1992).
[4] I. Affleck, A. W. W. Ludwig, and B. A. Jones, Phys. Rev. B **52**, 9528 (1995).
[5] A. Georges, G. Kotliar, W. Krauth, and M. J. Rozenberg, Rev. Mod. Phys. **68**, 13 (1996).
[6] M. Capone, M. Fabrizio, and E. Tosatti, Phys. Rev. Lett. **86**, 5361 (2001).
[7] M. Capone, M. Fabrizio, C. Castellani, and E. Tosatti, Science **296**, 2364 (2002).
[8] M. Fabrizio, A. F. Ho, L. De Leo, and G. E. Santoro, Phys. Rev. Lett. **91**, 246402 (2003).
[9] M. Capone, M. Fabrizio, C. Castellani, and E. Tosatti, cond-mat/0401090, Phys. Rev. Lett. (to be published).
[10] I. Affleck and A. W. W. Ludwig, Nucl. Phys. B **352**, 849 (1991).
[11] J. E. Han, cond-mat/0401104 (unpublished).
[12] K. G. Wilson, Rev. Mod. Phys. **47**, 773 (1975); H. R. Krishnamurthy, J. W. Wilkins, and K. G. Wilson, Phys. Rev. B **21**, 1003 (1980).
[13] In Ref. 8 there is a misprint concerning this point. Indeed the response to ST^x and ST^y fields are not singular, as erroneously written in that reference.
[14] C. Sire, C. M. Varma, and H. R. Krishnamurthy, Phys. Rev. B **48**, 13833 (1993).
[15] J. Gan, Phys. Rev. B **51**, 8287 (1995).
[16] T. A. Costi, A. C. Hewson, and V. Zlatić, J. Phys.: Condens. Matter **6**, 2519 (1994); R. Bulla, T. A. Costi and D. Vollhardt, Phys. Rev. B **64**, 045103 (2001).
[17] P. Nozières, J. Low Temp. Phys. **17**, 31 (1974).
[18] G. Zaránd and N. Andrei (unpublished).
[19] J. M. Maldacena and A. W. W. Ludwig, Nucl. Phys. B **506**, 565 (1997).
[20] We are indebted with G. Zaránd for this result.
[21] L. Mihály and A. Zawadowskii, J. Phys. (France) Lett. **39**, L-483 (1978), and references therein; A. Zawadowskii (unpublished).